

Efficient Learning Algorithms for Noisy Quantum State and Process Tomography

Chenyang Li,¹ Shengxin Zhuang,² Yukun Zhang,³ Jingbo B. Wang,² Xiao Yuan,^{3,*} Yusen Wu,^{1,†} and Chuan Wang^{1,‡}

¹*School of Artificial Intelligence, Beijing Normal University, Beijing, 100875, China*

²*Department of Physics, The University of Western Australia, Perth, WA 6009, Australia*

³*Center on Frontiers of Computing Studies, School of Computer Science, Peking University, Beijing 100871, China*

Efficiently characterizing large quantum states and processes is a central yet notoriously challenging task in quantum information science, as conventional tomography methods typically require resources that grow exponentially with system size. Here, we introduce a provably efficient and structure-agnostic learning framework for noisy n -qubit quantum circuits under generic noise with arbitrary noise strength. We first develop a sample-efficient learning algorithm for unital noisy quantum states. Building on this result, we extend the framework to quantum process tomography, obtaining a unified protocol applicable to both unital and non-unital channels. The resulting approach is input-agnostic and does not rely on assumptions about specific input distributions. Our theoretical analysis shows that both state and process learning require only polynomially many samples and polynomial classical post-processing in the number of qubits, while achieving near-unit success probability over ensembles generated by local random circuits. Numerical simulations of two-dimensional Hamiltonian dynamics further demonstrate the accuracy and robustness of the approach, including for structured circuits beyond the random-circuit setting assumed in the theoretical analysis. These results provide a scalable and practically relevant route toward characterizing large-scale noisy quantum devices, addressing a key bottleneck in the development of quantum technologies.

I. INTRODUCTION

Quantum computers are entering regimes beyond the reach of classical computational power [1–3]. Coherent manipulation of complex quantum states with hundreds of physical qubits has been demonstrated across multiple platforms, including trapped ions [4], neutral atom arrays [5], and superconducting qubit circuits [1, 2, 6]. As quantum hardware continues to scale in size and complexity, the ability to characterize quantum states and quantum processes becomes critical for advancing quantum error correction code [6, 7], quantum error mitigation [8, 9], and quantum algorithms [2, 10]. Among various approaches for characterizing quantum states and processes, quantum state tomography (QST) [11–16] and quantum process tomography (QPT) [17–19] stand as fundamental methods to reconstruct target quantum states and processes by leveraging measurement results.

The high dimensionality of Hilbert spaces imposes fundamental challenges on QST and QPT. Proven results indicate that, in the worst-case scenario, both tasks necessitate measuring a vast number of observables, incurring resource costs that grow exponentially relative to the system size [20–24]. Nevertheless, these “no-go” results do not rule out efficient algorithms in the average-case scenario. Indeed, by assuming specific input state distributions (e.g., locally flat distributions) or adopting relaxed learning objectives—such as quantum mean value learning or Hamiltonian learning—QPT and QST tasks can be rendered efficient in terms of both sample and classical post-processing complexity [25–54]. Despite this progress, efficiently characterizing quantum processes generated by noisy quantum computers remains an open problem. Specifically, a universally efficient framework capable of handling both unital and non-unital channels across arbitrary noise strengths and circuit depths has yet to be established; consequently, how to unify these disparate noise effects into a coherent learning framework remains a pivotal challenge. On the other hand, given the power of classical artificial-intelligence methods, it is natural to consider their application to complex QPT and QST tasks, such as neural-network models [55–58], tensor networks [59], diffusion models [60], and other approaches [61, 62]. However, these heuristic methods generally lack theoretical guarantees or may not handle QPT and QST in a noisy environment. These advances, together with the fundamental limitations discussed above, naturally raise a question: “*Can we efficiently learn a general noisy quantum process and quantum state?*”

In this paper, we answer this question by proposing a unified learning framework for both QPT and QST. Given the aforementioned “no-go” results for QPT and QST tasks [20–24], we do not expect any efficient learning protocols in the worst-case scenario. Here, we propose an efficient learning algorithm for the average-case regime by introducing a unified representation of noisy quantum processes and states. Specifically, let \mathcal{C} denote the target noisy quantum

* xiaoyuan@pku.edu.cn

† yusen.wu@bnu.edu.cn

‡ wangchuan@bnu.edu.cn

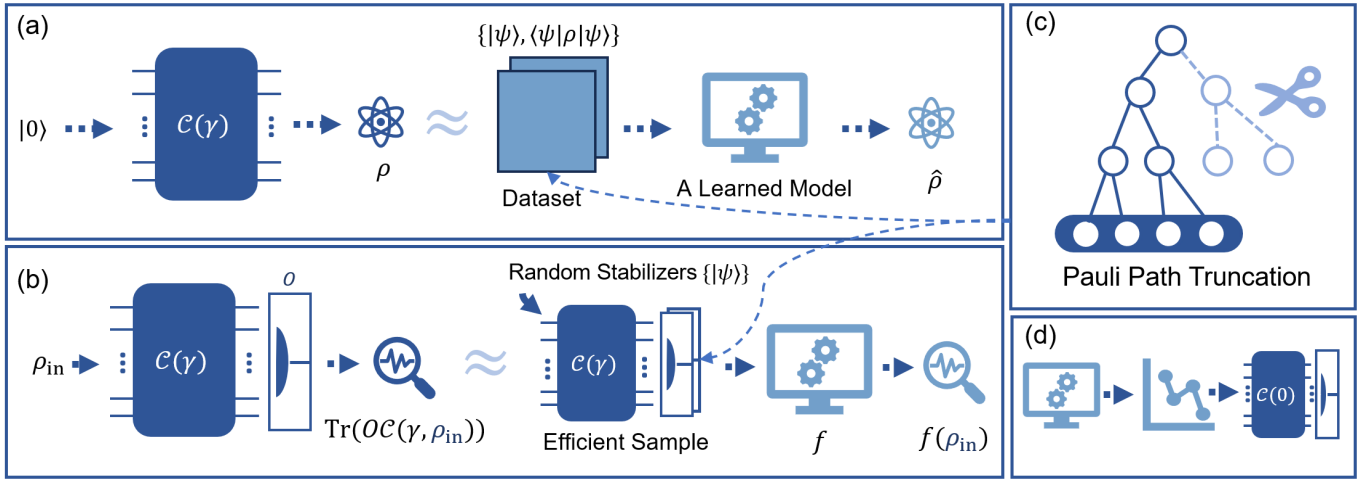


FIG. 1. (a) Illustration of the noisy quantum state learning, wherein a trained model $\hat{\rho}$ is generated by leveraging the adaptive measurement result from the target noisy quantum state ρ . (b) Depiction of the noisy quantum process learning. Here, the noisy quantum process $\mathcal{C}(\gamma)$ represents a d -depth quantum circuit with noise strength γ , and O represents an unknown measurement operator. The task is to learn a function f such that $|f(\cdot) - \text{Tr}[O\mathcal{C}(\gamma, \cdot)]| \leq \epsilon$ for all input quantum states ρ_{in} , with efficient sample complexity. (c) Outline of the fundamental principle underlying our learning algorithm. (d) The proposed learning algorithm can be applied to the quantum error mitigation task, more details are provided in Appendix G 1.

circuit. We establish a provably efficient learning algorithm for unital noisy quantum state $\rho = \mathcal{C}(|0^n\rangle\langle 0^n|)$ as a foundational step. Building upon this foundation, we show theoretically that the tomography task for any noisy quantum process $\text{Tr}(O\mathcal{C}(\cdot))$ accompanied by an unknown measurement O , regardless of whether the underlying noise channel is unital or non-unital, can be reduced to learning an unknown observable with the decomposition $\sum_{|P| \leq \mathcal{O}(1), P \in \{I, X, Y, Z\}^{\otimes n}} \alpha_P P$, where the coefficients $\alpha_P \in \mathbb{R}$. This observation reduces the learning space from 4^n to $\text{poly}(n)$, yielding an efficient learning algorithm when the quantum circuit suffers across the entire noise spectrum, from the noiseless limit ($\gamma = 0$) to constant noise levels ($\gamma = \Theta(1)$). The fundamental idea is illustrated in Fig. 1. Finally, we numerically benchmark our algorithm on noisy Hamiltonian dynamics driven by a two-dimensional lattice model [10]. The results demonstrate high accuracy for both QST and QPT tasks.

Functionally, our work establishes a “learning-theoretic dual” to classical simulation frameworks [63]. While classical simulation algorithms leverage the sparsity of the Pauli path integral to compute expectation values under the white-box assumption—requiring full knowledge of circuit parameters and noise strengths [64–66]—our protocol operates in a black-box setting. It reconstructs unknown processes solely from measurement data, requiring no prior information regarding the circuit architecture or specific noise levels. We reveal that the intrinsic properties of random quantum circuits directly imply a universally efficient sparse representation. Crucially, our algorithm’s complexity remains efficient across the entire noise regime $\gamma \in [0, 1)$ and is independent of circuit depth, offering a robust alternative to simulation methods that are often restricted to the deep-circuit or high-noise limits. Beyond being a dual to simulation, our approach significantly advances existing learning paradigms [67–69]. Unlike previous works that rely on specific input state distributions, unital dynamics or exponential scaling, our algorithm achieves input-agnostic prediction efficiently, remaining applicable to arbitrary input states and non-unital dynamics by leveraging the intrinsic sparse representation. Finally, we demonstrate the practical utility of this framework by applying the learned process models to quantum error mitigation, providing a pathway for noise-resilient quantum computing beyond mere verification. Detailed numerical validations for these applications are provided in the Appendix G 1.

II. NOISY QUANTUM CIRCUIT SETUP

In this paper, we consider an n -qubit noisy quantum process:

$$\mathcal{C} = \mathcal{E}^{\otimes n} \mathcal{C}_d \mathcal{E}^{\otimes n} \mathcal{C}_{d-1} \cdots \mathcal{E}^{\otimes n} \mathcal{C}_1, \quad (1)$$

where a local noise channel \mathcal{E} (either unital or non-unital) with noise strength γ is applied uniformly throughout the circuit. The circuit has depth d , and each layer \mathcal{C}_i comprises two-qubit gates acting on arbitrary pairs, with each gate sampled uniformly from a local 2-design unitary group. Crucially, our learning protocol is *agnostic* to

circuit connectivity and applicable to arbitrary architectures—including standard parameterized brickwork structures, quantum cellular automata, and tree-structured circuits [70–72]—provided that each two-qubit gate satisfies the local 2-design assumption. By interleaving unitary layers \mathcal{C}_i with i.i.d. tensor-product noise $\mathcal{E}^{\otimes n}$, this framework serves as a canonical model for quantum verification. Specifically, it provides the theoretical foundation for validating tasks that are proven to be classically hard, such as quantum advantage experiments [1, 10]. A rigorous definition of the model’s topological generality is provided in Appendix B.

III. NOISY QUANTUM STATE TOMOGRAPHY

We first consider the noisy QST task in the context of unital-noise environment, where the objective is to construct a classical approximation $\hat{\rho}$ of the output state $\rho = \mathcal{C}(|0^n\rangle\langle 0^n|)$ such that $\|\rho - \hat{\rho}\|_1 \leq \epsilon$. In this regime, we expand the noisy state $\mathcal{C}(|0^n\rangle\langle 0^n|)$ in the Pauli basis: $\mathcal{C}(|0^n\rangle\langle 0^n|) = \sum_{P \in \{I, X, Y, Z\}^{\otimes n}} \alpha_P P$, where $\alpha_P = 2^{-n} \text{Tr}[P \mathcal{C}(|0^n\rangle\langle 0^n|)]$. Given the random ensemble formed by $\{\mathcal{C}_1, \dots, \mathcal{C}_d\}$, it can be proven that the coefficients α_P of high-weight Pauli terms decay exponentially, leading to an effectively sparse representation. The detailed proof can be found in the Appendix D 2. Specifically, we show that the noisy quantum state $\rho = \mathcal{C}(|0^n\rangle\langle 0^n|)$ admits a sparse approximation $\hat{\rho} = \sum_{|P| \leq l'} \alpha_P P$ such that $\|\rho - \hat{\rho}\|_1 \leq \epsilon$ with success probability at least $1 - \delta$ over the ensemble. Here, the truncation weight is given by

$$l' = \mathcal{O}\left(\frac{\log(1/\epsilon\delta)}{\log[2(1-\gamma)^{-2}]}\right). \quad (2)$$

This implies that the noisy quantum state can be effectively truncated to ‘low-weight’ Pauli operators. We note that this result holds for any noise strength $\gamma \in [0, 1]$ [73], thereby unifying previous results given in Refs. [64, 65, 74]. Since all ‘low-weight’ Pauli operators $|P| \leq l'$ can be pre-enumerated, the classical shadow method [43] becomes a natural candidate for estimating the ‘low-weight’ coefficients α_P with $|P| \leq l'$, achieving a sample complexity of $\mathcal{O}(l' \epsilon^{-2})$.

Nevertheless, the classical shadow method may not extend directly to quantum process tomography tasks. To implement a ‘unified’ learning approach for both QST and QPT tasks, we provide another method to estimate coefficients α_P from the quantum randomized measurement results. We generate a dataset $\{|\psi_j\rangle = \otimes_{i=1}^n |\psi_{i,j}\rangle, v_j = \langle \psi_j | \rho | \psi_j \rangle\}_{j=1}^{N_{\text{data}}}$ by drawing each single-qubit stabilizer $|\psi_{i,j}\rangle$ uniformly sampled from the set $\text{Stab} = \{|0\rangle, |1\rangle, |+\rangle, |-\rangle, |y+\rangle, |y-\rangle\}$. Here, the quantum state overlap $v_j = \langle \psi_j | \rho | \psi_j \rangle$ can be efficiently obtained by using SWAP-test method [75] or standard classical shadow [43]. All involved coefficients are thus estimated by $\hat{\alpha}_P = \frac{3^{|P|}}{N_{\text{data}}} \sum_{j=1}^{N_{\text{data}}} v_j \langle \psi_j | P | \psi_j \rangle$. The in-depth explanation of the learning Algorithm is provided in Appendix D 3. We note that the above learning approach is efficient in both sample and computational complexity (classical post-processing), and a rigorous result is summarized as follows.

Theorem 1 (Noisy Quantum State Learning). *For any noisy quantum state ρ prepared by Eq. 1 with the unital-noise channel, there exists a learning algorithm that outputs an estimator $\hat{\rho} = \sum_{|P| \leq l'} \alpha_P P$ such that $\|\rho - \hat{\rho}\|_1 \leq \epsilon$ with success probability $\geq 1 - \delta$ over the choice of the quantum circuit. The sample complexity is $\mathcal{O}\left(\left(\frac{1}{\epsilon}\right)^{\frac{1}{\log[2/(1-\gamma)]}}\right)$ and the classical post-processing complexity is $\mathcal{O}\left(n \cdot \left(\frac{1}{\epsilon}\right)^{\frac{1}{\log[2/(1-\gamma)]}}\right)$, where the noise strength parameter γ takes value from $[0, 1)$.*

Compared with other verification methods, such as the classical simulation approaches [64], our learning algorithm does not require prior knowledge of the value of γ . Furthermore, the algorithm is applicable to any noise strength $\gamma \in [0, 1)$, extending well beyond previous classical simulation frameworks that are only efficient when $\gamma = \Omega(1)$. On the other hand, the sample (computational) complexity decreases as γ increases. This implies that the hardness of learning noisy states is a smooth function of γ , exhibiting a fundamental different from the computational hardness results in random circuit sampling, which feature a clear complexity transition between $\gamma = 0$ and $\gamma = \Omega(1)$.

IV. NOISY QUANTUM PROCESS TOMOGRAPHY

Now we generalize above analysis and learning method to QPT tasks. Given an n -qubit observable $O = \sum_{k=1}^M c_k P_k$ composed of $M = \text{poly}(n)$ Pauli terms, the goal is to learn a function f from measurement results. This function predicts the expectation value for arbitrary valid input state ρ_{in} , satisfying $|f(\rho_{\text{in}}) - \text{Tr}[O \mathcal{C}(\rho_{\text{in}})]| \leq \epsilon$. Here, we do not restrict the locality of O , actually, it may include global Pauli terms with $|P_k| = \mathcal{O}(n)$.

TABLE I. Comparisons of our results with related previous studies on solving the quantum process learning problem, focusing on input distribution, target channel, sample complexity and classical post-processing complexity

| Algorithm | Input Distribution | Channel | Sample Complexity (N_{data}) | Classical Runtime |
|-------------------|---------------------------|---|---|--|
| Huang et al. [67] | Locally flat distribution | CPTP | $2^{\mathcal{O}(\log(n) \log(1/\epsilon))}$ | $\mathcal{O}(N_{\text{data}})$ |
| Chen et al. [68] | Product state | CPTP | $\min\left(\frac{2^{\mathcal{O}(n)}}{\epsilon^2}, n^{\mathcal{O}(\log \epsilon^{-1}/\log \frac{1}{1-\eta})}\right) \cdot \log \frac{1}{\delta}$ | $\mathcal{O}(N_{\text{data}})$ |
| Raza et al. [69] | No restriction | Pauli Channel | $\mathcal{O}\left(\sqrt{n} \log(M) (\log \frac{1}{\epsilon \delta})^{3/2} \epsilon^{-3}\right)$ | $\mathcal{O}(N_{\text{data}} \cdot 4^n)$ |
| Our Result | No restriction | Quantum Circuit with i.i.d. single-qubit noise | $\mathcal{O}\left(6^{l'} \cdot \epsilon^{-2} \log(1/\delta)\right)$ | $\mathcal{O}(n \cdot N_{\text{data}})$ |

Note: $\eta \in (0, 1)$ relates to input distribution; M is the number of Pauli terms within observable O . $l' = \mathcal{O}\left(\frac{\log(\|O\|_{\mathbb{F}}^2/\epsilon\delta)}{\log(\Lambda \log(1-\gamma)^{-2})}\right)$ is the Pauli weight truncation threshold, representing the dominant term in the exponent.

Inspired by the aforementioned noisy QST task, we propose an efficient learning algorithm for the QPT task, surprisingly, we find our learning algorithm is even applicable to non-unital noise channels in the QPT tasks. In detail, we focus on the Heisenberg picture from the perspective of the operator evolution, transforming the objective from learning the quantum channel $\text{Tr}[OC(\cdot)]$ to learn the dual operator $\mathcal{C}^\dagger(O)$. Assuming the input states are drawn from a structured ensemble, such as locally flat or general product distributions, Refs. [67, 68] propose learning a Hermitian operator by truncating all high-weight Pauli terms. This approach yields a learning algorithm with a sample complexity of $\mathcal{O}(n^{\log(1/\epsilon)})$, which crucially depends on the specific input-state ensemble. To decouple learning efficiency from the input state distribution, Ref. [69] leverages an online learning framework with a sample complexity of $\tilde{\mathcal{O}}(\sqrt{n})$. However, it incurs an $\mathcal{O}(4^n)$ classical post-processing overhead to update and recover the associated Choi matrix. This exponentially increasing runtime limits its scalability for large-scale systems. Here, we overcome the above barriers by leveraging a universally efficient sparse representation, naturally induced by the intrinsic structure of random quantum circuits. This compact representation is independent of both noise strength and circuit depth. We show that our algorithm is sample- and computationally efficient at predicting outcomes for arbitrary input states, including highly entangled states that explicitly violate the distributional assumptions of prior work. A more detailed comparison is provided in Table I and the SI material A.

Similar to the QST task, our fundamental strategy relies on finding an effective representation $\sum_{|P| \leq l'} \beta_P P$, which approximates the target $\mathcal{C}^\dagger(O)$ in terms of the normalized Frobenius norm. To ensure independence from the input state distribution, the core idea is to introduce a ‘‘decay coefficient’’ such that $\beta_P \propto c^{|P|}$ for some constant $c < 1$. While Refs. [67, 68] utilized specific input state ensembles and Refs. [64, 65] relied on constant-level noise channels to induce this decay, we demonstrate that this phenomenon is naturally inherent in locally random circuits, across a noise strength γ ranging from 0 to a constant, and it is independent of the quantum circuit depth.

For unital noise channel, the analysis is the same to QPT tasks. Regarding the non-unital noise, we leverage the decomposition technique which factorizes the channel into a depolarizing component and a suitable (non-physical) linear map \mathcal{E}' . Crucially, the adjoint of this effective map is unital ($\mathcal{E}'^\dagger(I) = I$), ensuring that the operator evolution remains bounded in the Frobenius norm. This structural property facilitates rigorous truncation bounds even for non-unital physical noise, ensuring that $\mathcal{C}^\dagger(O)$ retains a sparse Pauli structure amenable to efficient learning. We derive a generalized scaling law for the process truncation: with probability $\geq 1 - \delta$, there exists a truncated process $\mathcal{C}^{(l')\dagger}(O) = \sum_{|P| \leq l'} \beta_P P$ with Pauli weight at most l' such that the approximation error is bounded by ϵ . Here

$$l' = \mathcal{O}\left(\frac{\log(\|O\|_{\mathbb{F}}^2/\epsilon\delta)}{\log(\Lambda(1-\gamma)^{-2})}\right), \quad (3)$$

where $\Lambda > 1$ is the structural scrambling constant dependent on the noise type, and $\|O\|_{\mathbb{F}}^2 = 2^{-n} \text{Tr}[OO^\dagger]$ represents the squared normalized Frobenius norm. The detailed proof is provided in the Appendix E2. Similar to the noisy QST task, reconstructing $\mathcal{C}^{(l')\dagger}(O)$ proceeds from the data set

$$\mathcal{D}_{\text{QPT}} = \{|\psi_j\rangle = \otimes_{i=1}^n |\psi_{i,j}\rangle, \phi_j = \text{Tr}[OC(|\psi_j\rangle\langle\psi_j|)]\}_{j=1}^{N_{\text{data}}},$$

where $|\psi_{i,j}\rangle$ is a single-qubit stabilizer randomly sampled from the set Stab , and ϕ_j denotes the output of the target quantum process. Thus, coefficients β_P can be learned efficiently via $\beta_P = \frac{3^{|P|}}{N_{\text{data}}} \sum_{i=1}^{N_{\text{data}}} \phi_j \langle\psi_i| P |\psi_i\rangle$.

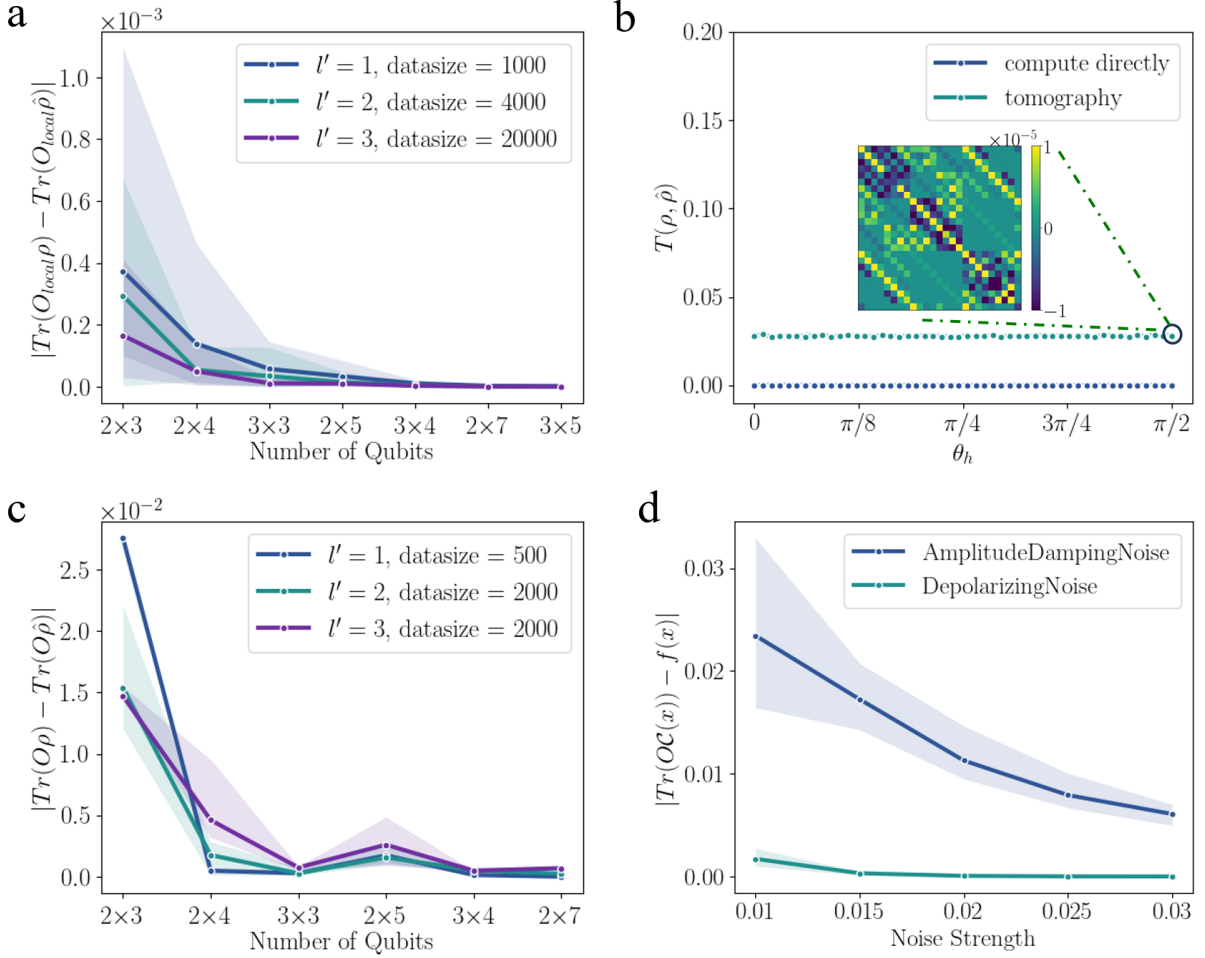


FIG. 2. (a) QST results for various numbers of qubits and l' . Each circuit is 20 layers accompanied by depolarizing noise of strength 0.02 and fixed $\theta_h = \frac{\pi}{4}$. The grid illustrates the 3×5 2D transverse field Ising model. (b). Learning of the ρ generated by sweeping θ_h from 0 to $\frac{\pi}{2}$; the circuit size 2×5 , 45 layers, depolarizing noise strength 0.02. The heat-map shows a 25×25 sub-matrix of the matrix $\langle i | (\rho - \hat{\rho}) | j \rangle$ at $\theta_h = \frac{\pi}{2}$, where basis $i, j \in \{0, 1\}^n$ (the full matrix in Appendix G3). (c). QPT results for different qubit numbers and l' , where the circuit depth is 5 layers and the depolarizing noise strength is 0.01. (d). QPT for the 2×5 system under 2 kinds of noise and other settings identical to c.

From the above algorithm, it can be observed that the computational overhead primarily stems from two sources: (1) the sampling complexity N_{data} , (2) and the complexity of classical post-processing. Both of these costs depend on the number of P , which in turn is governed by how many legal Pauli paths are retained, in other words, the number of Pauli operators P with non-zero parameter β_P contained in $\mathcal{C}^{(l')\dagger}(O)$, where the weight of P is given by l' . Therefore, a rough estimate of the number of legal paths N_s is $\mathcal{O}(n^{l'})$. For $\epsilon = 1/n$, the number of legal paths becomes $\mathcal{O}(n^{\log n})$, incurring quasi-polynomial sampling and post-processing complexity.

However, we can tighten the bound to retain only $e^{\mathcal{O}(l')}$ legal paths. We rely on a volume conservation argument: the total weight of the process (sum of squared coefficients) is bounded by $\mathcal{O}(1)$ due to the trace-preserving nature of the dynamics. Conversely, the 2-design scrambling imposes a lower bound on the contribution of each valid path: a path of weight l carries a variance of at least $(1/15)^l$. By focusing on the terminal Pauli weight l' that captures the dominant dynamics, the total number of such valid paths cannot exceed the inverse of this minimum contribution. This yields the tight bound $N_s \leq 15^{\mathcal{O}(l')} = e^{\mathcal{O}(l')}$. While simulation algorithms must track the entire path history [64, 74], our approach leverages the fact that all preceding evolution and noise effects are implicitly contracted within the learned coefficients $\{\beta_P\}$, allowing the complexity to be governed solely by the terminal Pauli weight l' which remains independent of the circuit depth d . We conclude the main results in the following Theorem. The proof is given in Appendix E4.

Theorem 2 (Noisy Quantum Process Learning). *For any noisy quantum process \mathcal{C} given by Eq. 1, and an n -qubit*

observable $O = \sum_{k=1}^M c_k Q_k$ with $M = \text{poly}(n)$, there exists a learning algorithm that learns a function f from measurement results, satisfying $|f(\rho_{in}) - \text{Tr}[OC(\rho_{in})]| \leq \epsilon$ with success probability $\geq 1 - \delta$. The sample complexity and the classical post-processing complexity are $\text{poly}(n, 1/\epsilon)$ for any noise strength γ .

To contextualize our contribution, we compare the complexity and applicability of our protocol with state-of-the-art quantum learning algorithms in Table I.

V. NUMERICAL RESULTS

Although our theoretical results rely on the randomness assumption, we numerically verify that our learning algorithm remains highly efficient for a broader class of circuits, including those with specific structure, such as noisy quantum dynamical processes. This demonstrates the broad practical applicability of our approach. Specifically, we benchmark the noisy Hamiltonian dynamics of 2D transverse-field Ising model given by $H = -J \sum_{\langle q,p \rangle} Z_q Z_p + h \sum_q X_q$. The time evolution is implemented via Trotterization as a sequence of $R_{ZZ}(\theta_J = -\pi/2)$ and $R_X(\theta_h)$ gates [10]. Using Qulacs [76], we simulate noisy circuits under two conditions: i.i.d. single-qubit depolarizing noise ($p = 0.02$) for the unital case, and a mixture of depolarizing and amplitude damping for the non-unital case. Our simulations cover system sizes up to 3×5 qubits and 20 layers, a scale that occupies 16 GB RAM.

The numerical results are presented in Fig. 2, where shaded areas indicate the outcome range over 10 trials. Consistent with Theorems 1 and 2, Figs. 2 (a) and (c) show that the reconstruction error stabilizes at large system sizes, confirming the localized nature of the learning problem. Figs. 2 (b) and (d) further demonstrate robustness against parameter variations and non-unital noise; interestingly, stronger noise yields higher accuracy, reflecting the tighter Pauli weight confinement. Beyond sample efficiency, our method enables extreme memory compression: a 14-qubit state description is reduced from 8 GB (full matrix) to just 1 KB (sparse coefficients).

Beyond tomography, our framework enables practical Quantum Error Mitigation (QEM). As detailed in Appendix G1, we apply the learned models to perform input-agnostic Zero-Noise Extrapolation (ZNE) on the 2D Ising model. By fitting the expectation values across varying noise scales, we effectively recover the noise-free dynamics with high precision, demonstrating the utility of our algorithm for near-term device calibration.

VI. DISCUSSION

Efficiently characterizing noisy quantum states and processes is a fundamental challenge. We propose a provably efficient learning algorithm handling both unital and non-unital channels, generalizing prior art to arbitrary input states. Notably, our algorithm maintains sample and runtime efficiency across the entire noise spectrum, from the noiseless limit ($\gamma = 0$) to constant noise levels ($\gamma = \Theta(1)$). Crucially, this efficiency extends to arbitrary circuit depths, as the preceding evolution history is implicitly contracted within the terminal coefficients to be learned.

Functionally, our work serves as a “learning-theoretic dual” to classical simulation [63]. While simulation algorithms predict outcomes by aggregating dominant Pauli paths based on known circuit parameters [64, 66, 77], our approach identifies these statistically significant terms directly from measurement data, solving the inverse problem without requiring priors on circuit depth or architecture [78]. This offers a complementary benchmarking perspective to standard certification methods [13].

Several open problems remain for future study. First, while our main theorems establish average-case efficiency, we also derive a sample complexity lower bound for the worst-case scenario (see Appendix F), underscoring the inherent hardness of QST tasks in such cases. This raises the question: can we theoretically characterize the efficiency boundaries of QST and QPT tasks? Furthermore, we show that sample complexity is a smooth function of the noise strength γ , exhibiting a fundamental difference from the computational hardness results in random circuit sampling, which feature a sudden complexity transition. Exploring the formal relationship between learning complexity and computational complexity remains an intriguing direction. Finally, extending our i.i.d. analysis to gate-dependent noise models is crucial for characterizing more practical quantum hardware.

Acknowledgments

This work is supported by National Natural Science Foundation of China (NSFC) Grants (No. 62501060, No. 62461160263, No. 12361161602 and No. 62131002), NSAF (Grant No. U2330201), Beijing Natural Science Foundation Z250004, Beijing Science and Technology Planning Project (Grant No. Z25110100810000) Quantum Science and Technology-National Science and Technology Major Project (2023ZD0300200), and the High-performance Computing Platform of Peking University and Pawsey Supercomputing Research Centre.

-
- [1] Frank Arute, Kunal Arya, Ryan Babbush, Dave Bacon, Joseph C Bardin, Rami Barends, Rupak Biswas, Sergio Boixo, Fernando GSL Brandao, David A Buell, et al. Quantum supremacy using a programmable superconducting processor. *Nature*, 574(7779):505–510, 2019.
- [2] Alexis Morvan, B Villalonga, X Mi, S Mandra, A Bengtsson, PV Klimov, Z Chen, S Hong, C Erickson, IK Drozdov, et al. Phase transitions in random circuit sampling. *Nature*, 634(8033):328–333, 2024.
- [3] Han-Sen Zhong, Hui Wang, Yu-Hao Deng, Ming-Cheng Chen, Li-Chao Peng, Yi-Han Luo, Jian Qin, Dian Wu, Xing Ding, Yi Hu, et al. Quantum computational advantage using photons. *Science*, 370(6523):1460–1463, 2020.
- [4] Jacob Smith, Aaron Lee, Philip Richerme, Brian Neyenhuis, Paul W Hess, Philipp Hauke, Markus Heyl, David A Huse, and Christopher Monroe. Many-body localization in a quantum simulator with programmable random disorder. *Nature Physics*, 12(10):907–911, 2016.
- [5] Simon J Evered, Dolev Bluvstein, Marcin Kalinowski, Sepehr Ebadi, Tom Manovitz, Hengyun Zhou, Sophie H Li, Alexandra A Geim, Tout T Wang, Nishad Maskara, et al. High-fidelity parallel entangling gates on a neutral-atom quantum computer. *Nature*, 622(7982):268–272, 2023.
- [6] Rajeev Acharya, Laleh Aghababaie-Beni, Igor Aleiner, Trond I Andersen, Markus Ansmann, Frank Arute, Kunal Arya, Abraham Asfaw, Nikita Astrakhantsev, Juan Atalaya, et al. Quantum error correction below the surface code threshold. *arXiv preprint arXiv:2408.13687*, 2024.
- [7] Sergey Bravyi, Andrew W Cross, Jay M Gambetta, Dmitri Maslov, Patrick Rall, and Theodore J Yoder. High-threshold and low-overhead fault-tolerant quantum memory. *Nature*, 627(8005):778–782, 2024.
- [8] Youngseok Kim, Christopher J. Wood, Theodore J. Yoder, Seth T. Merkel, Jay M. Gambetta, Kristan Temme, and Abhinav Kandala. Scalable error mitigation for noisy quantum circuits produces competitive expectation values. *Nature Physics*, 19(5):752–759, 2023.
- [9] Thomas E O’Brien, G Anselmetti, Fotios Gkritis, VE Elfving, Stefano Polla, William J Huggins, Oumarou Oumarou, Kostyantyn Kechedzhi, Dmitry Abanin, Rajeev Acharya, et al. Purification-based quantum error mitigation of pair-correlated electron simulations. *Nature Physics*, 19(12):1787–1792, 2023.
- [10] Youngseok Kim, Andrew Eddins, Sajant Anand, Ken Xuan Wei, Ewout Van Den Berg, Sami Rosenblatt, Hasan Nayfeh, Yantao Wu, Michael Zaletel, Kristan Temme, and Abhinav Kandala. Evidence for the utility of quantum computing before fault tolerance. *Nature*, 618(7965):500–505, June 2023.
- [11] K Banaszek, M Cramer, and D Gross. Focus on quantum tomography. *New Journal of Physics*, 15(12):125020, December 2013.
- [12] Robin Blume-Kohout. Optimal, reliable estimation of quantum states. *New Journal of Physics*, 12(4):043034, April 2010.
- [13] Jens Eisert, Dominik Hangleiter, Nathan Walk, Ingo Roth, Damian Markham, Rhea Parekh, Ulysse Chabaud, and Elham Kashefi. Quantum certification and benchmarking. *Nature Reviews Physics*, 2(7):382–390, June 2020.
- [14] David Gross, Yi-Kai Liu, Steven T. Flammia, Stephen Becker, and Jens Eisert. Quantum state tomography via compressed sensing. *Physical Review Letters*, 105(15):150401, October 2010.
- [15] Z. Hradil. Quantum-state estimation. *Physical Review A*, 55(3):R1561–R1564, March 1997.
- [16] G. Mauro D’Ariano, Matteo G.A. Paris, and Massimiliano F. Sacchi. Quantum tomography. In *Advances in Imaging and Electron Physics*, volume 128, pages 205–308. Elsevier, 2003.
- [17] Isaac L. Chuang and M. A. Nielsen. Prescription for experimental determination of the dynamics of a quantum black box. *Journal of Modern Optics*, 44(11-12):2455–2467, November 1997.
- [18] G. M. D’Ariano and P. Lo Presti. Quantum tomography for measuring experimentally the matrix elements of an arbitrary quantum operation. *Physical Review Letters*, 86(19):4195–4198, May 2001.
- [19] M. Mohseni, A. T. Rezakhani, and D. A. Lidar. Quantum-process tomography: Resource analysis of different strategies. *Physical Review A*, 77(3):032322, March 2008.
- [20] Sitan Chen, Jerry Li, Brice Huang, and Allen Liu. Tight bounds for quantum state certification with incoherent measurements. In *2022 IEEE 63rd Annual Symposium on Foundations of Computer Science (FOCS)*, pages 1205–1213, Denver, CO, USA, October 2022. IEEE.
- [21] Jeongwan Haah, Robin Kothari, Ryan O’Donnell, and Ewin Tang. Query-optimal estimation of unitary channels in diamond distance. In *2023 IEEE 64th Annual Symposium on Foundations of Computer Science (FOCS)*, pages 363–390, November 2023.
- [22] Jeongwan Haah, Aram W. Harrow, Zhengfeng Ji, Xiaodi Wu, and Nengkun Yu. Sample-optimal tomography of quantum states. *IEEE Transactions on Information Theory*, pages 1–1, 2017.
- [23] Ryan O’Donnell and John Wright. Efficient quantum tomography. In *Proceedings of the Forty-Eighth Annual ACM Symposium on Theory of Computing*, pages 899–912, Cambridge MA USA, June 2016. ACM.
- [24] Aadil Oufkir. Sample-optimal quantum process tomography with non-adaptive incoherent measurements. In *2023 IEEE International Symposium on Information Theory (ISIT)*, pages 1919–1924, June 2023.
- [25] Scott Aaronson and Sabee Grewal. Efficient tomography of non-interacting fermion states. (arXiv:2102.10458), February 2023.
- [26] Anurag Anshu, Srinivasan Arunachalam, Tomotaka Kuwahara, and Mehdi Soleimanifar. Sample-efficient learning of quantum many-body systems. In *2020 IEEE 61st Annual Symposium on Foundations of Computer Science (FOCS)*, pages 685–691, Durham, NC, USA, November 2020. IEEE.
- [27] Srinivasan Arunachalam, Sergey Bravyi, Arkopal Dutt, and Theodore J. Yoder. Optimal algorithms for learning quantum

- phase states. (arXiv:2208.07851), May 2023.
- [28] Eyal Bairey, Itai Arad, and Netanel H. Lindner. Learning a local hamiltonian from local measurements. *Physical Review Letters*, 122(2):020504, January 2019.
- [29] Liangyu Che, Chao Wei, Yulei Huang, Dafa Zhao, Shunzhong Xue, Xinfang Nie, Jun Li, Dawei Lu, and Tao Xin. Learning quantum hamiltonians from single-qubit measurements. *Physical Review Research*, 3(2):023246, June 2021.
- [30] Senrui Chen, Sisi Zhou, Alireza Seif, and Liang Jiang. Quantum advantages for pauli channel estimation. *Physical Review A*, 105(3):032435, March 2022.
- [31] Marcus Cramer, Martin B. Plenio, Steven T. Flammia, Rolando Somma, David Gross, Stephen D. Bartlett, Olivier Landon-Cardinal, David Poulin, and Yi-Kai Liu. Efficient quantum state tomography. *Nature Communications*, 1(1):149, December 2010.
- [32] Steven T. Flammia and Joel J. Wallman. Efficient estimation of pauli channels. *ACM Transactions on Quantum Computing*, 1(1):1–32, December 2020.
- [33] Steven T. Flammia and Ryan O’Donnell. Pauli error estimation via population recovery. *Quantum*, 5:549, September 2021.
- [34] Valentin Gebhart, Raffaele Santagati, Antonio Andrea Gentile, Erik M. Gauger, David Craig, Natalia Ares, Leonardo Banchi, Florian Marquardt, Luca Pezzè, and Cristian Bonato. Learning quantum systems. *Nature Reviews Physics*, February 2023.
- [35] Christopher E Granade, Christopher Ferrie, Nathan Wiebe, and D G Cory. Robust online hamiltonian learning. *New Journal of Physics*, 14(10):103013, October 2012.
- [36] Sabee Grewal, Vishnu Iyer, William Kretschmer, and Daniel Liang. Improved stabilizer estimation via bell difference sampling. (arXiv:2304.13915), March 2024.
- [37] Sabee Grewal, Vishnu Iyer, William Kretschmer, and Daniel Liang. Low-stabilizer-complexity quantum states are not pseudorandom. *LIPICs, Volume 251, ITCS 2023*, 251:64:1–64:20, 2023.
- [38] David Gross, Sepehr Nezami, and Michael Walter. Schur–weyl duality for the clifford group with applications: Property testing, a robust hudson theorem, and de finetti representations. *Communications in Mathematical Physics*, 385(3):1325–1393, August 2021.
- [39] Andi Gu, Lukasz Cincio, and Patrick J. Coles. Practical black box hamiltonian learning. *Nature Communications*, 15(1):312, January 2024.
- [40] Jeongwan Haah, Robin Kothari, and Ewin Tang. Optimal learning of quantum hamiltonians from high-temperature gibbs states. In *2022 IEEE 63rd Annual Symposium on Foundations of Computer Science (FOCS)*, pages 135–146, Denver, CO, USA, October 2022. IEEE.
- [41] Dominik Hangleiter, Ingo Roth, Jonáš Fuksa, Jens Eisert, and Pedram Roushan. Robustly learning the hamiltonian dynamics of a superconducting quantum processor. *Nature Communications*, 15(1):9595, November 2024.
- [42] Hsin-Yuan Huang, Yu Tong, Di Fang, and Yuan Su. Learning many-body hamiltonians with heisenberg-limited scaling. *Physical Review Letters*, 130(20):200403, May 2023.
- [43] Hsin-Yuan Huang, Richard Kueng, and John Preskill. Predicting many properties of a quantum system from very few measurements. *Nature Physics*, 16(10):1050–1057, October 2020.
- [44] Ching-Yi Lai and Hao-Chung Cheng. Learning quantum circuits of some T gates. *IEEE Transactions on Information Theory*, 68(6):3951–3964, June 2022.
- [45] B. P. Lanyon, C. Maier, M. Holzäpfel, T. Baumgratz, C. Hempel, P. Jurcevic, I. Dhand, A. S. Buyskikh, A. J. Daley, M. Cramer, M. B. Plenio, R. Blatt, and C. F. Roos. Efficient tomography of a quantum many-body system. *Nature Physics*, 13(12):1158–1162, December 2017.
- [46] Zhi Li, Liujun Zou, and Timothy H. Hsieh. Hamiltonian tomography via quantum quench. *Physical Review Letters*, 124(16):160502, April 2020.
- [47] Ashley Montanaro. Learning stabilizer states by bell sampling. (arXiv:1707.04012), July 2017.
- [48] Cambyse Rouzé and Daniel Stilck França. Learning quantum many-body systems from a few copies. *Quantum*, 8:1319, April 2024.
- [49] Daniel Stilck França, Liubov A. Markovich, V. V. Dobrovitski, Albert H. Werner, and Johannes Borregaard. Efficient and robust estimation of many-qubit hamiltonians. *Nature Communications*, 15(1):311, January 2024.
- [50] Ewout Van Den Berg, Zlatko K. Mineev, Abhinav Kandala, and Kristan Temme. Probabilistic error cancellation with sparse pauli–lindblad models on noisy quantum processors. *Nature Physics*, 19(8):1116–1121, August 2023.
- [51] Wenjun Yu, Jinzhao Sun, Zeyao Han, and Xiao Yuan. Robust and efficient hamiltonian learning. *Quantum*, 7:1045, June 2023.
- [52] Assaf Zubida, Elad Yitzhaki, Netanel H. Lindner, and Eyal Bairey. Optimal short-time measurements for hamiltonian learning. 2021.
- [53] Yusen Wu, Yukun Zhang, Chuan Wang, and Xiao Yuan. Hamiltonian dynamics learning: A scalable approach to quantum process characterization. *arXiv preprint arXiv:2503.24171*, 2025.
- [54] Yusen Wu, Bujiao Wu, Jingbo Wang, and Xiao Yuan. Quantum phase recognition via quantum kernel methods. *Quantum*, 7:981, 2023.
- [55] Roger G Melko, Giuseppe Carleo, Juan Carrasquilla, and J Ignacio Cirac. Restricted boltzmann machines in quantum physics. *Nature Physics*, 15(9):887–892, 2019.
- [56] Anirudh Acharya, Theodore Kypraios, and Mădălin Guță. A comparative study of estimation methods in quantum tomography. *Journal of Physics A: Mathematical and Theoretical*, 52(23):234001, 2019.
- [57] Marc Wanner, Laura Lewis, Chiranjib Bhattacharyya, Devdatt Dubhashi, and Alexandru Gheorghiu. Predicting ground

- state properties: Constant sample complexity and deep learning algorithms. In *Advances in Neural Information Processing Systems*, volume 37, pages 33962–34024, 2024.
- [58] Yehui Tang, Hao Xiong, Nianzu Yang, Tailong Xiao, and Junchi Yan. Towards LLM4QPE: Unsupervised pretraining of quantum property estimation and a benchmark. In *The Twelfth International Conference on Learning Representations*, 2024.
- [59] Giacomo Torlai, Christopher J. Wood, Atithi Acharya, Giuseppe Carleo, Juan Carrasquilla, and Leandro Aolita. Quantum process tomography with unsupervised learning and tensor networks. *Nature Communications*, 14(1):2858, 2023.
- [60] Tang Yehui, Long Mabiao, and Yan Junchi. Quadim: A conditional diffusion model for quantum state property estimation. In *The Thirteenth International Conference on Learning Representations*, 2025.
- [61] Yusen Wu, Bujiao Wu, Yanqi Song, Xiao Yuan, and Jingbo Wang. Learning the complexity of weakly noisy quantum states. In *The Thirteenth International Conference on Learning Representations*, 2025.
- [62] Yuxuan Du, Min-Hsiu Hsieh, and Dacheng Tao. Efficient learning for linear properties of bounded-gate quantum circuits. *Nature Communications*, 16(1):3790, 2025.
- [63] Elies Gil-Fuster, Casper Gyurik, Adrian Perez-Salinas, and Vedran Dunjko. On the relation between trainability and dequantization of variational quantum learning models. In Y. Yue, A. Garg, N. Peng, F. Sha, and R. Yu, editors, *International Conference on Representation Learning*, volume 2025, pages 24069–24093, 2025.
- [64] Dorit Aharonov, Xun Gao, Zeph Landau, Yunchao Liu, and Umesh Vazirani. A Polynomial-Time Classical Algorithm for Noisy Random Circuit Sampling. In *Proceedings of the 55th Annual ACM Symposium on Theory of Computing*, pages 945–957, Orlando FL USA, June 2023. ACM.
- [65] Yuguang Shao, Fuchuan Wei, Song Cheng, and Zhengwei Liu. Simulating Noisy Variational Quantum Algorithms: A Polynomial Approach. *Physical Review Letters*, 133(12):120603, September 2024.
- [66] Thomas Schuster, Chao Yin, Xun Gao, and Norman Y. Yao. A polynomial-time classical algorithm for noisy quantum circuits. *Physical Review X*, 15(4):041018, 2025.
- [67] Hsin-Yuan Huang, Sitan Chen, and John Preskill. Learning to Predict Arbitrary Quantum Processes. *PRX Quantum*, 4(4):040337, December 2023.
- [68] Sitan Chen, Jaume de Dios Pont, Jun-Ting Hsieh, Hsin-Yuan Huang, Jane Lange, and Jerry Li. Predicting quantum channels over general product distributions. (arXiv:2409.03684), September 2024.
- [69] Asad Raza, Matthias C. Caro, Jens Eisert, and Sumeet Khatri. Online learning of quantum processes. (arXiv:2406.04250), June 2024.
- [70] Leo Zhou, Sheng-Tao Wang, Soonwon Choi, Hannes Pichler, and Mikhail D. Lukin. Quantum approximate optimization algorithm: Performance, mechanism, and implementation on near-term devices. *Physical Review X*, 10(2):021067, 2020.
- [71] Abhinav Kandala, Antonio Mezzacapo, Kristan Temme, Maika Takita, Markus Brink, Jerry M. Chow, and Jay M. Gambetta. Hardware-efficient variational quantum eigensolver for small molecules and quantum magnets. *Nature*, 549(7671):242–246, 2017.
- [72] Harper R. Grimsley, Sophia E. Economou, Edwin Barnes, and Nicholas J. Mayhall. An adaptive variational algorithm for exact molecular simulations on a quantum computer. *Nature Communications*, 10(1):3007, 2019.
- [73] Our result does not cover the trivial case $\gamma = 1$.
- [74] Armando Angrisani, Alexander Schmidhuber, Manuel S. Rudolph, M. Cerezo, Zoë Holmes, and Hsin-Yuan Huang. Classically estimating observables of noiseless quantum circuits. *Physical Review Letters*, 135(17):170602, October 2025.
- [75] Harry Buhrman, Richard Cleve, John Watrous, and Ronald De Wolf. Quantum fingerprinting. *Physical review letters*, 87(16):167902, 2001.
- [76] Yasunari Suzuki, Yoshiaki Kawase, Yuya Masumura, Yuria Hiraga, Masahiro Nakadai, Jiabao Chen, Ken M. Nakanishi, Kosuke Mitarai, Ryosuke Imai, Shiro Tamiya, Takahiro Yamamoto, Tennin Yan, Toru Kawakubo, Yuya O. Nakagawa, Yohei Ibe, Youyuan Zhang, Hirotsugu Yamashita, Hikaru Yoshimura, Akihiro Hayashi, and Keisuke Fujii. Qulacs: A fast and versatile quantum circuit simulator for research purpose. *Quantum*, 5:559, 2021.
- [77] Armando Angrisani, Antonio A. Mele, Manuel S. Rudolph, M. Cerezo, and Zoe Holmes. Simulating quantum circuits with arbitrary local noise using pauli propagation. (arXiv:2501.13101), January 2025.
- [78] Senrui Chen, Yunchao Liu, Matthew Otten, Alireza Seif, Bill Fefferman, and Liang Jiang. The learnability of pauli noise. *Nature Communications*, 14(1):52, 2023.
- [79] Jarrod R. McClean, Sergio Boixo, Vadim N. Smelyanskiy, Ryan Babbush, and Hartmut Neven. Barren plateaus in quantum neural network training landscapes. *Nature Communications*, 9(1):4812, 2018.
- [80] M. Cerezo, Akira Sone, Tyler Volkoff, Lukasz Cincio, and Patrick J. Coles. Cost function dependent barren plateaus in shallow parametrized quantum circuits. *Nature Communications*, 12(1):1791, 2021.
- [81] Huangjun Zhu, Richard Kueng, Markus Grassl, and David Gross. The clifford group fails gracefully to be a unitary 4-design. (arXiv:1609.08172), 2016.
- [82] Antonio Anna Mele. Introduction to haar measure tools in quantum information: A beginners tutorial. *Quantum*, 8:1340, 2024.
- [83] Jonas Haferkamp, Philippe Faist, Naga B. T. Kothakonda, Jens Eisert, and Nicole Yunger Halpern. Linear growth of quantum circuit complexity. *Nature Physics*, 18(5):528–532, 2022.
- [84] Ryan Babbush, Robbie King, Sergio Boixo, William Huggins, Tanuj Khattar, Guang Hao Low, Jarrod R. McClean, Thomas O’Brien, and Nicholas C. Rubin. The grand challenge of quantum applications, 2025.
- [85] Jeongwan Haah, Robin Kothari, and Ewin Tang. Learning quantum hamiltonians from high-temperature gibbs states and real-time evolutions. *Nature Physics*, 20(6):1027–1031, June 2024.
- [86] Hsin-Yuan Huang, Yunchao Liu, Michael Broughton, Isaac Kim, Anurag Anshu, Zeph Landau, and Jarrod R. McClean.

- Learning Shallow Quantum Circuits. In *Proceedings of the 56th Annual ACM Symposium on Theory of Computing*, pages 1343–1351, June 2024.
- [87] Emanuel Knill, Dietrich Leibfried, Rolf Reichle, Joe Britton, R Brad Blakestad, John D Jost, Chris Langer, Roe Ozeri, Signe Seidelin, and David J Wineland. Randomized benchmarking of quantum gates. *Physical Review A*, 77(1):012307, 2008.
- [88] Jonas Helsen, Xiao Xue, Lieven MK Vandersypen, and Stephanie Wehner. A new class of efficient randomized benchmarking protocols. *npj Quantum Information*, 5(1):1–9, 2019.
- [89] Senrui Chen, Wenjun Yu, Pei Zeng, and Steven T. Flammia. Robust shadow estimation. *PRX Quantum*, 2(3):030348, 2021.
- [90] Michael A Nielsen and Isaac L Chuang. *Quantum Computation and Quantum Information*, volume 2. Cambridge university press Cambridge, 2001.
- [91] Peter W Shor. Fault-tolerant quantum computation. In *Proceedings of 37th Conference on Foundations of Computer Science*, pages 56–65. IEEE, 1996.
- [92] Joel J Wallman and Joseph Emerson. Noise tailoring for scalable quantum computation via randomized compiling. *Physical Review A*, 94(5):052325, 2016.
- [93] Joel J. Wallman and Joseph Emerson. Noise tailoring for scalable quantum computation via randomized compiling. *Phys. Rev. A*, 94:052325, Nov 2016.
- [94] Samson Wang, Enrico Fontana, Marco Cerezo, Kunal Sharma, Akira Sone, Lukasz Cincio, and Patrick J Coles. Noise-induced barren plateaus in variational quantum algorithms. *Nature communications*, 12(1):1–11, 2021.
- [95] Zhenyu Cai, Ryan Babbush, Simon C. Benjamin, Suguru Endo, William J. Huggins, Ying Li, Jarrod R. McClean, and Thomas E. O’Brien. Quantum error mitigation. *Reviews of Modern Physics*, 95(4):045005, 2023.
- [96] Abhinav Kandala, Kristan Temme, Antonio D. Córcoles, Antonio Mezzacapo, Jerry M. Chow, and Jay M. Gambetta. Error mitigation extends the computational reach of a noisy quantum processor. *Nature*, 567(7749):491–495, 2019.
- [97] Suguru Endo, Simon C. Benjamin, and Ying Li. Practical quantum error mitigation for near-future applications. *Physical Review X*, 8(3):031027, 2018.

APPENDIX

Appendix A: Comparison with other works

Tables II and III contrast our framework with prominent quantum learning paradigms, highlighting significant disparities in resource scaling and applicability. Our work establishes a provably efficient regime that—under the assumption of random noisy circuit dynamics—fundamentally distinguishes its resource requirements from existing methods.

1. Generalization and Noise Scope

As detailed in Table II, our framework introduces crucial extensions in two key dimensions relative to prior art.

A central theoretical contribution of our framework is the unified treatment of both i.i.d. single-qubit unital and non-unital noise channels. This stands in sharp contrast to complexity results derived for the n -qubit Pauli channel model [69]. While their framework captures global correlations, it remains inherently restricted to unital dynamics, whereas our approach tackles the distinct challenge of generic non-unitality. The capacity of our framework to handle non-unital CPTP maps is essential for modeling realistic hardware decoherence, such as amplitude damping, which remains inaccurate under unital approximations.

Complementing this noise universality, our QPT algorithm yields a strictly *input-agnostic* characterization. Unlike protocols that rely on rotationally symmetric input distributions [67] or specific product-state ensembles [68], our approach operates independently of the input distribution. This guarantees predictive robustness for arbitrary input states, effectively bypassing the distribution-shift limitations inherent in previous works. Our framework remains valid even for input states that violate standard distribution assumptions, such as highly entangled states (see Appendix G 2 for preliminary numerical tests on entangled inputs).

TABLE II. **Comparison of Applicability Constraints.** We compare the allowed input distributions and the supported noise models.

| work | input distribution | Channel |
|-------------------|---|-------------------------------------|
| Huang et al. [67] | at most polynomially far from a locally flat distribution | General CPTP map |
| Chen et al. [68] | Product state, $\ \Gamma\ _{op} \leq 1 - \eta$ | General CPTP map |
| Raza et al. [69] | No restriction | n -qubit Pauli channel |
| Our Work | No restriction | Arbitrary i.i.d. single-qubit noise |

Note: The parameter Γ represents the Pauli second-moment matrix of the input state distribution.

2. Resource Scaling and Efficiency Regime

The Table III shows a comparison between our theoretical work with other related works. For constant accuracy ϵ , the sample complexity in our algorithm is proportional only to a factor exponential in L , which is independent of n . This contrasts sharply with the method of Ref. [69], which suffers from a $\mathcal{O}(\sqrt{n})$ polynomial dependency on the system size n , and an intractable $\mathcal{O}(4^n)$ classical runtime bottleneck inherent to standard shadow tomography protocols when estimating general channels.

When considering high precision requirements, such as setting the accuracy ϵ to $\frac{1}{n}$, our complexity grows only polynomially with n . This provides a substantial advantage over the approaches of Ref. [67] and Ref. [68], which incur a quasi-polynomial dependence ($n^{\mathcal{O}(\log n)}$ or $2^{\mathcal{O}(\log n \log(1/\epsilon))}$) due to their reliance on methods that scale with the logarithm of the system size in the exponent. Our ability to bypass this quasi-polynomial scaling stems from the statistical decay properties inherent to random noisy circuits. This model-induced constraint (captured by $\Lambda > 1$) confines the learned system to a low-weight Pauli subspace, ensuring genuinely polynomial scaling in n for accuracy $\epsilon = \frac{1}{\text{poly}(n)}$.

TABLE III. **Comparison of Resource Complexity.** Complexity bounds for learning an n -qubit process to accuracy ϵ with failure probability δ . N_{data} denotes the dataset size. Note that our classical runtime is linear in n , and sample complexity is strictly polynomial (independent of n for constant error).

| Work | Classical Runtime | Sample Complexity (N_{data}) |
|-------------------|--|--|
| Huang et al. [67] | $\mathcal{O}(N_{\text{data}})$ | $2^{\mathcal{O}(\log(n) \log(1/\epsilon))}$ |
| Chen et al. [68] | $\mathcal{O}(N_{\text{data}})$ | $\min\left(\frac{2^{\mathcal{O}(n)}}{\epsilon^2}, n^{\mathcal{O}\left(\frac{\log \epsilon^{-1}}{\log \frac{1}{1-\eta}}\right)}\right) \cdot \log \frac{1}{\delta}$ |
| Raza et al. [69] | $\mathcal{O}(N_{\text{data}} \cdot 4^n)$ | $\mathcal{O}\left(\frac{\sqrt{n} \log(M) (\log(1/(\epsilon\delta)))^{\frac{3}{2}}}{\epsilon^3}\right)$ |
| Our Work | $\mathcal{O}(n \cdot N_{\text{data}})$ | $\mathcal{O}\left(6^{l'} \cdot \epsilon^{-2} \log(1/\delta)\right)$ |

Note: Here, $\eta \in (0, 1)$ is related to the input distribution; M is the number of Observables. And $l' = \mathcal{O}\left(\frac{\log(\|O\|_{\mathbb{F}}^2/\epsilon\delta)}{\log(\Lambda \log(1-\gamma)^{-2})}\right)$ is the Pauli weight truncation threshold seeing in Lemma 4 and denoted as the dominant term in the exponent.

Appendix B: Structure and Applicability of the noisy circuit in this work

We emphasize that the quantum process studied serves as a standard model with wide and practical applications, especially in the Near-Term Intermediate Scale Quantum (NISQ) era. This appendix details the topological definitions, generality, and practical relevance of the quantum circuit model investigated.

1. Topological Definition and Model Generality

The studied noisy quantum process \mathcal{C} adopts a layered structure, representing a large class of quantum circuits:

$$\mathcal{C} = \mathcal{E}^{\otimes n} \mathcal{C}_d \mathcal{E}^{\otimes n} \mathcal{C}_{d-1} \cdots \mathcal{E}^{\otimes n} \mathcal{C}_1, \quad (\text{B1})$$

in which a γ -strength local noise channel \mathcal{E} (unital or non-unital) is applied uniformly throughout the circuit. The quantum circuit depth is d , and each layer \mathcal{C}_i consists of two-qubit gates acting on arbitrary qubit pairs, where each gate is uniformly sampled from a local 2-design unitary group. Each layer \mathcal{C}_i can realise variational algorithms such as VQE, QAOA or quantum neural networks [70–72], while the local noise assumption $\mathcal{E}^{\otimes n}$ captures typical NISQ imperfections. The local 2-design assumption is an extremely weak condition, where quantum neural network models are typical cases [79, 80], and even Clifford gates satisfy such an assumption [81]. We note that if an ensemble follows a $(t+1)$ -design, it must follow the t -design property [82]. As a result, this assumption is very general and covers a large amount of NISQ algorithms related to 'randomly initial parameters' and 'classical optimizations' [79, 80].

The circuit model is formally defined below using graph-theoretic definitions:

Definition 1 (Architecture, restatement of Ref. [83]). An architecture is a directed acyclic graph that contains $R \in \mathbb{Z}_{>0}$ vertices (gates). Two edges (qubits) enter each vertex, and two edges exit. Two typical examples are listed below:

- A brickwork is the architecture of any circuit formed as follows. Apply a string of two-qubit gates: $U_{1,2} \otimes U_{3,4} \otimes \cdots \otimes U_{n-1,n}$. Then apply a staggered string of gates. Perform this pair of steps T times in total, using possibly different gates each time.
- A staircase is the architecture of any circuit which applies a stepwise string of two-qubit gates: $U_{n,n-1} U_{n-2,n-1} \cdots U_{2,1}$. Repeat this process T times, using possibly different gates each time.

Here, the quantum circuit layer \mathcal{C}_i may adopt any architecture, and *we note that our learning algorithm can be applied to any geometrical architecture*, and thus covers a large class of noisy quantum circuits, especially for those used in NISQ algorithms.

Definition 2 (Random Quantum Circuit, restatement of Ref. [83]). Let G denote an arbitrary architecture. A probability distribution can be induced over the architecture- G circuits as follows: for each vertex in G , draw a gate Haar-randomly from $SU(4)$. Then contract the unitaries along the edges of G . Each circuit so constructed is called a random quantum circuit.

Definition 3 (Random noisy quantum circuit). Let \tilde{G} denote an arbitrary architecture. A probability distribution can be induced over the architecture- \tilde{G} circuits as follows: for each vertex in \tilde{G} , draw a gate Haar-randomly from $SU(4)$ and an i.i.d single-qubit noisy channel. Then contract the unitaries along the edges of \tilde{G} . Each circuit so constructed is called a random noisy quantum circuit.

The guarantee is a high-probability bound ($\geq 1 - \delta$) over random circuit ensemble defined in Definition. 3. Furthermore, we numerically demonstrate that our learning algorithm can successfully handle a noisy Hamiltonian dynamics approach, where the underlying quantum circuit does not possess the locally random property.

2. Importance for Quantum Benchmarking and Learning

To design powerful quantum algorithms, such as quantum neural network models and related states, a benchmarking algorithm is necessary [1, 84]; otherwise, one may not verify and check the correctness of the implemented quantum algorithm. Following this logic, a large amount of quantum learning algorithms are proposed for quantum state (process) tomography, Hamiltonian learning[85], shallow circuit learning[86], quantum gate tomography, and other quantum benchmarking algorithms. **To the best of our knowledge, this is the first efficient learning algorithm for noisy state and process tomography**, providing an efficient tool for verifying the output of the implemented quantum algorithms on NISQ devices.

3. The Gate-Independent Noise Model

We utilize the gate-independent noise model, which posits that the detrimental effects impacting quantum operations are uniform across all fundamental gates, irrespective of their specific type or physical implementation. This simplifying assumption is widely adopted due to several key factors:

- **Theoretical Tractability:** Adopting a gate-independent noise assumption allows researchers to advance the development and analysis of error correction protocols and fault-tolerant methodologies without needing to incorporate the intricate details of gate-specific noise characteristics[87–89]. This uniformity facilitates the derivation of universal results and theoretical performance bounds [90].
- **Practical Approximations:** In particular quantum systems—especially those featuring highly calibrated gates acting on the same number of qubits and employing standardized control mechanisms—the variability of noise across different gates can be negligible[1, 91]. In these instances, the gate-independent noise model serves as a tenable approximation, streamlining analysis without substantially compromising precision.
- **Alignment with Noise Conversion Methods (Twirling):** Techniques like Pauli twirling are routinely applied to convert complicated physical noise channels into simpler, diagonal forms in the Pauli basis[78, 92]. The resulting channel can often be effectively approximated as gate-independent, thereby conforming to the model’s postulates.

The gate-independent noise model thus furnishes a foundational framework for comprehending error propagation and engineering correction strategies. We identify the robust depiction of gate-dependent noise, which typically manifests in larger, more intricate quantum architectures, as a significant avenue for future exploration.

Appendix C: Norm definition

Definition 4 (Schatten τ -Norm). *The Schatten τ -norm of a matrix A is defined as $\|A\|_\tau = (\sum_i \nu_i^\tau)^{\frac{1}{\tau}}$, where ν_i is the singular value of A and τ is a positive integer. Note that $\|A\|_1 = \text{Tr}[\sqrt{AA^\dagger}]$, and $\|A\|_2$ coincides with the Frobenius norm.*

Definition 5 (The Squared Normalized Frobenius Norm). *Suppose the matrix $A = \sum_P \alpha_P P$, with $P \in \mathcal{P}_n = \{X, Y, Z, I\}^{\otimes n}$, its squared normalized Frobenius norm is defined by $\|A\|_{\mathbb{F}}^2 = 2^{-n} \text{Tr}[(\sum_P \alpha_P P)(\sum_P \alpha_P P)^\dagger] = \sum_P |\alpha_P|^2$.*

Definition 6 (Hamming Weight of Pauli Operators). *Suppose P represents an n -qubit (normalized) Pauli operator, then its Hamming weight $|P|$ is defined as the number of qubits that are non-trivially acted by P .*

Appendix D: Learning a Quantum state

The representation of noisy quantum state are presented in this section, together with further implementation details of the QST algorithm.

1. Noisy Quantum State

In this section, we will give an unified representation of noisy quantum state under Pauli propagation.

Lemma 1 (Unified Representation of Noisy Quantum State). *Let the noisy quantum state $\rho = \mathcal{C}(|0^n\rangle\langle 0^n|)$ with $\mathcal{C} = \mathcal{E}^{\otimes n}\mathcal{C}_d\mathcal{E}^{\otimes n}\mathcal{C}_{d-1}\cdots\mathcal{E}^{\otimes n}\mathcal{C}_1$ representing a d -depth noisy quantum circuit, where $\mathcal{C}_i(\cdot) = C_i(\cdot)C_i^\dagger$ is a unitary channel consisting of a layer of two-qubit gates, and \mathcal{E} is a unital single-qubit noise channel with strength parameter γ . Then the noisy quantum state ρ can be represented by the Pauli path integral, that is*

$$\rho = \sum_{s \in \tilde{\mathcal{P}}_n^{\otimes(d+1)}} (1 - \gamma)^{|s|} \Phi(\mathcal{C}, s) s_d, \quad (\text{D1})$$

where the $n(d+1)$ -qubit operator $s = s_0 s_1 \cdots s_d$, $\tilde{\mathcal{P}}_n = \{I/\sqrt{2}, X/\sqrt{2}, Y/\sqrt{2}, Z/\sqrt{2}\}^{\otimes n}$. The Pauli weight $|s|$ represents the number of non-identity operators in $s \in \tilde{\mathcal{P}}_n^{\otimes(d+1)}$. The coefficient

$$\Phi(\mathcal{C}, s) = \text{Tr}(s_d \mathcal{C}_d(s_{d-1})) \cdots \text{Tr}(s_1 \mathcal{C}_1(s_0)) \langle 0^n | s_0 | 0^n \rangle. \quad (\text{D2})$$

We prove it by describing three types of noisy channels, which are depolarizing noise, single-qubit Pauli noise, and non-unital noise.

a. Depolarizing Noise

The property of depolarizing noise $\mathcal{E}_{\text{depo}}$ is that

$$\begin{aligned} \mathcal{E}_{\text{depo}}(I) &= I, \\ \mathcal{E}_{\text{depo}}(X) &= (1 - \gamma)X, \\ \mathcal{E}_{\text{depo}}(Y) &= (1 - \gamma)Y, \\ \mathcal{E}_{\text{depo}}(Z) &= (1 - \gamma)Z, \end{aligned} \quad (\text{D3})$$

so that

$$\begin{aligned} \rho &= \sum_{s \in \tilde{\mathcal{P}}_n^{\otimes(d+1)}} s_d \text{Tr}(s_d \mathcal{E}_{\text{depo}}^{\otimes n} \mathcal{C}_d(s_{d-1})) \cdots \text{Tr}(s_1 \mathcal{E}_{\text{depo}}^{\otimes n} \mathcal{C}_1(s_0)) \langle 0^n | s_0 | 0^n \rangle \\ &= \sum_{s \in \tilde{\mathcal{P}}_n^{\otimes(d+1)}} (1 - \gamma)^{|s|} s_d \Phi(\mathcal{C}, s), \end{aligned} \quad (\text{D4})$$

where $|s|$ means the number of non-identities in s .

b. Pauli Noise

We use \mathcal{E} to denote the noise function. Pauli noise $\mathcal{E}_{\text{Pauli}}$ is

$$\mathcal{E}_{\text{Pauli}}(\rho) = \gamma_1 \rho + \gamma_2 X \rho X^\dagger + \gamma_3 Y \rho Y^\dagger + \gamma_4 Z \rho Z^\dagger, \quad (\text{D5})$$

where $\gamma_1 + \gamma_2 + \gamma_3 + \gamma_4 = 1$. The Pauli noise has the property that

$$\begin{aligned} \mathcal{E}_{\text{Pauli}}(I) &= (\gamma_1 + \gamma_2 + \gamma_3 + \gamma_4)I = I, \\ \mathcal{E}_{\text{Pauli}}(X) &= (\gamma_1 + \gamma_2 - \gamma_3 - \gamma_4)X = (1 - 2(\gamma_3 + \gamma_4))X, \\ \mathcal{E}_{\text{Pauli}}(Y) &= (\gamma_1 - \gamma_2 + \gamma_3 - \gamma_4)Y = (1 - 2(\gamma_2 + \gamma_4))Y, \\ \mathcal{E}_{\text{Pauli}}(Z) &= (\gamma_1 - \gamma_2 - \gamma_3 + \gamma_4)Z = (1 - 2(\gamma_2 + \gamma_3))Z. \end{aligned} \quad (\text{D6})$$

So the Pauli Channel can be written as

$$\begin{aligned}\rho &= \sum_{s \in \tilde{\mathcal{P}}_n^{d+1}} s_d \text{Tr}(s_d \mathcal{E}_{\text{Pauli}}^{\otimes n} \mathcal{C}_d(s_{d-1})) \cdots \text{Tr}(s_1 \mathcal{E}_{\text{Pauli}}^{\otimes n} \mathcal{C}_1(s_0)) \text{Tr}(s_0 |0^n\rangle \langle 0^n|) \\ &= \sum_{s \in \tilde{\mathcal{P}}_n^{d+1}} (1 - 2(\gamma_3 + \gamma_4))^{|s|_x} (1 - 2(\gamma_2 + \gamma_4))^{|s|_y} (1 - 2(\gamma_2 + \gamma_3))^{|s|_z} s_d \Phi(\mathcal{C}, s),\end{aligned}\tag{D7}$$

where $|s|_{\tilde{P}}$ denotes the number of \tilde{P} in s . Without loss of generality, to simplify the presentation while maintaining a conservative upper bound on path decay, we consider a uniform noise rate $\gamma = \min\{\gamma_2 + \gamma_3, \gamma_2 + \gamma_4, \gamma_3 + \gamma_4\}$, where $0 \leq \gamma < 1$. This substitution ensures that the decay factor for each Pauli component is upper-bounded by a uniform term $(1 - \gamma)^{|s|}$, where $|s|$ is the total weight of the Pauli string. For brevity, we denote $\rho = \sum_{s \in \tilde{\mathcal{P}}_n^{d+1}} (1 - \gamma)^{|s|} s_d \Phi(\mathcal{C}, s)$ in the subsequent discussion, which does not alter the analysis of the learning algorithm.

Techniques like Pauli twirling are employed to transform complex unital channels into diagonal forms on the Pauli basis [78, 93]. In the following, we utilize the Pauli noise channel to represent the unital channel. Thus, complete the proof of Lemma 1.

2. State Learning Truncation

Ref. [64] proved that sampling from a depolarizing channel reduces to fitting a constant number l of Pauli paths. We generalize this observation to single-qubit Pauli noise that admits a sparse Pauli-path expansion.

According to Lemma 1, for an arbitrary i.i.d single-qubit noise, the output state is approximated by

$$\hat{\rho} = \sum_{|s_d| \leq l', s_d \in \tilde{\mathcal{P}}_n} \alpha_{s_d} s_d = \sum_{s \in \tilde{\mathcal{P}}_n^{d+1}, |s| \leq l} (1 - \gamma)^{|s|} s_d \Phi(\mathcal{C}, s).\tag{D8}$$

In other words, we can learn the finite number of the legal Pauli paths to get a $\hat{\rho}$ satisfying $\|\rho - \hat{\rho}\|_1 < \epsilon$, where $\|A\|_1$ is the Schatten 1-norm of A . The formal statement and proof are given in Lemma 2.

Lemma 2 (The unital noisy state truncation). *Let the noisy quantum state $\rho = \mathcal{C}(|0^n\rangle \langle 0^n|)$ with $\mathcal{C} = \mathcal{E}^{\otimes n} \mathcal{C}_d \mathcal{E}^{\otimes n} \mathcal{C}_{d-1} \cdots \mathcal{E}^{\otimes n} \mathcal{C}_1$ representing a d -depth noisy quantum circuit, where \mathcal{C}_i is a layer of two-qubit Haar random quantum gates. When the noise is unital, there exists a density matrix $\hat{\rho} = \sum_{|s_d| \leq l', s_d \in \tilde{\mathcal{P}}_n} \alpha_{s_d} s_d$ such that*

$$\|\rho - \hat{\rho}\|_1 < \epsilon_1,\tag{D9}$$

where coefficients $\alpha_{s_d} \in \mathbb{R}$ and $l' = \mathcal{O}\left(\frac{\log(\epsilon_1^{-1} \delta_1^{-1})}{\log(2/(1-\gamma)^2)}\right)$ with the success probability $\geq 1 - \delta_1$.

Proof. Firstly, we consider the Frobenius norm:

$$\begin{aligned}\Delta &:= \|\rho - \hat{\rho}\|_2 \\ &= \sqrt{\text{Tr} \left(\left(\sum_{|s| > l} (1 - \gamma)^{|s|} s_d \Phi(\mathcal{C}, s) \right) \left(\sum_{|s| > l} (1 - \gamma)^{|s|} s_d \Phi(\mathcal{C}, s) \right)^\dagger \right)} \\ &= \sqrt{\text{Tr} \left(\sum_{|s| > l} \sum_{|s'| > l} (1 - \gamma)^{|s'| + |s|} s_d s_d'^\dagger \Phi(\mathcal{C}, s) \Phi(\mathcal{C}, s') \right)} \\ &= \sqrt{\sum_{|s| > l} \sum_{|s'| > l} (1 - \gamma)^{|s'| + |s|} \Phi(\mathcal{C}, s) \Phi(\mathcal{C}, s') \text{Tr} \left(s_d s_d'^\dagger \right)}.\end{aligned}\tag{D10}$$

The above equation illustrates the constraint that the error of $\hat{\rho}$ receives from the sum of a series of constants. The orthogonality of the circuit, which is

$$\mathbb{E}[\Phi(\mathcal{C}, s) \Phi(\mathcal{C}, s')] = 0.\tag{D11}$$

Furthermore, we have

$$\begin{aligned}
\mathbb{E}_{\mathcal{C}}(\Delta^2) &= \mathbb{E}_{\mathcal{C}} \left(\sum_{|s|>l} \sum_{|s'|>l} (1-\gamma)^{|s'|+|s|} \Phi(\mathcal{C}, s) \Phi(\mathcal{C}, s') \text{Tr} \left(s_d s_d^\dagger \right) \right) \\
&= \mathbb{E}_{\mathcal{C}} \left(\sum_{|s|>l} (1-\gamma)^{2|s|} \Phi(\mathcal{C}, s)^2 \text{Tr} \left(s_d s_d^\dagger \right) \right) \\
&= \mathbb{E}_{\mathcal{C}} \left(\sum_{|s|>l} (1-\gamma)^{2|s|} \Phi(\mathcal{C}, s)^2 \right) \\
&= \sum_{k>l} (1-\gamma)^{2k} W_k.
\end{aligned} \tag{D12}$$

The second line is obtained via the orthogonality mentioned above. The third line uses the property that $\text{Tr} \left(s_d s_d^\dagger \right) = 1$ where s_d is the combination of the normalized Pauli operators. The last line denotes $W_k = \mathbb{E}_{\mathcal{C}, |s|=k} \Phi(\mathcal{C}, s)^2$. For W_k , it can be written as follows

$$\begin{aligned}
W_k &= \mathbb{E}_{\mathcal{C}, |s|=k} \Phi(\mathcal{C}, s)^2 \\
&= \mathbb{E}_{\mathcal{C}, |s|=k} \left(\text{Tr}(s_d \mathcal{C}_d(s_{d-1})) \cdots \text{Tr}(s_1 \mathcal{C}_1(s_0)) \text{Tr}(s_0 |0^n\rangle \langle 0^n|) \right)^2 \\
&= 2^{-n} \mathbb{E}_{\mathcal{C}_d} \text{Tr}(s_d \mathcal{C}_d(s_{d-1}))^2 \cdots \mathbb{E}_{\mathcal{C}_1} \text{Tr}(s_1 \mathcal{C}_1(s_0))^2.
\end{aligned} \tag{D13}$$

The third line assumes that every \mathcal{C}_i is independent respectively, and $\text{Tr}(s_0 |0^n\rangle \langle 0^n|) = \frac{1}{\sqrt{2^n}}$. For unital noises, using the equation

$$\mathbb{E}_{U \sim \text{SU}(4)} \text{Tr}(xU(y))^2 = \mathbb{E}_{U \sim \text{SU}(4)} \text{Tr}(xUyU^\dagger)^2 = \begin{cases} 1, & x = y = I^{\otimes 2}/2, \\ 0, & x = I^{\otimes 2}/2, y \neq I^{\otimes 2}/2, \\ 0, & x \neq I^{\otimes 2}/2, y = I^{\otimes 2}/2, \\ \frac{1}{15}, & \text{else.} \end{cases} \tag{D14}$$

We observe that certain Pauli paths contribute 0 to the circuit; these are termed illegal Pauli paths.

For $k = 0$, $W_k = 1$, where the Pauli path s consists of identity operators.

For $k \in (0, d]$, $W_k = 0$.

For $k \geq d + 1$, we can bound W_k by focusing on every term, which is in the form of $\mathbb{E}_{\mathcal{C}_i} \text{Tr}(s_i \mathcal{C}_i(s_{i-1}))^2$.

Noting that each \mathcal{C}_i is a layer of two-qubit gates, \mathcal{C}_i is equal to the multiplication of $\mathcal{C}_i^{(j)}$, where j indexes the two-qubit gates in the layer and N_g is the total number of such gates in a layer. So

$$\begin{aligned}
\mathbb{E}_{\mathcal{C}_i} \text{Tr}(s_i \mathcal{C}_i(s_{i-1}))^2 &= \bigotimes_j^{N_g} \mathbb{E}_{\mathcal{C}_i^{(j)}} \left(\text{Tr}(s_i^{(j)} s_i^{(j+1)} \mathcal{C}_i^{(j)} s_{i-1}^{(j)} s_{i-1}^{(j+1)} \mathcal{C}_i^{(j)\dagger}) \right)^2 \\
&\leq \left(\frac{1}{15} \right)^{\frac{|s_i|}{2}}.
\end{aligned} \tag{D15}$$

The last line is due to that one gate introduces at most 2 non-identity Pauli operators to the path when $k \geq d + 1$. Since any single gate can be accountable for at most four non-identity entries (two incoming and two outgoing), the number of two-qubit gates that actually contribute to the suppression factor $1/15$ is at least $\frac{|s|}{4}$.

In that case, Eq. D13 is bounded by:

$$W_k \leq \left(\frac{1}{15} \right)^{\frac{k}{4}} \left(\frac{1}{2} \right)^n. \tag{D16}$$

Since the $\left(\frac{1}{15} \right)^{\frac{k}{4}}$ is a decreasing sequence, we can get $\sum_{k>l} \left(\frac{1}{15} \right)^{\frac{k}{4}} \leq \frac{15^{-l/4}}{\sqrt[4]{15}-1}$.

By inequality between Schatten τ -norms, we have

$$\|\rho\|_1 \leq 2^{n/2} \|\rho\|_2. \tag{D17}$$

So the $\mathbb{E}_{\mathcal{C}}(\|\rho - \hat{\rho}\|_1^2)$ is bounded as:

$$\begin{aligned}
\mathbb{E}_{\mathcal{C}}(\|\rho - \hat{\rho}\|_1^2) &\leq 2^n \mathbb{E}_{\mathcal{C}}(\Delta^2) \\
&= 2^n \sum_{k>l} (1-\gamma)^{2k} W_k \\
&\leq 2^n \sum_{k>l} (1-\gamma)^{2l} W_k \\
&\leq 2^n (1-\gamma)^{2l} 2^{-n} \sum_{k>l} \left(\frac{1}{15}\right)^{\frac{k}{4}} \\
&\leq \left(\frac{(1-\gamma)^2}{\sqrt[4]{15}}\right)^l \frac{1}{\sqrt[4]{15}-1}.
\end{aligned} \tag{D18}$$

By Markov's inequality,

$$\mathbb{P}(\|\rho - \hat{\rho}\|_1^2 \geq \epsilon_1^2) \leq \frac{\mathbb{E}(\|\rho - \hat{\rho}\|_1)}{\epsilon_1^2} = \delta_1. \tag{D19}$$

Hence, choosing $l' = \mathcal{O}(l) = \frac{\log\left(\frac{1}{\sqrt[4]{15}-1} \epsilon_1^{-2} \delta_1^{-1}\right)}{\log\left(\frac{\sqrt[4]{15}}{1-\gamma}\right)} = \mathcal{O}\left(\frac{\log(\epsilon_1^{-1} \delta_1^{-1})}{\log(2/(1-\gamma)^2)}\right)$, yields $\|\rho - \hat{\rho}\|_1 \leq \epsilon_1$ with success probability $\geq 1 - \delta_1$. □

3. Algorithm of Learning a Quantum State

For the first problem, there are several ways to get the $\hat{\rho}$. The sections following introduce 2 methods, including computing directly by classical shadow [43], and a way of learning alpha based on Ref.[86]

a. Compute Directly

As shown before, $\rho = \sum_{s_d \in \mathcal{P}_n} \alpha_{s_d} s_d$, where $s_d \in \tilde{\mathcal{P}}_n$. In that case,

$$\begin{aligned}
\alpha_{s_d} &= \text{Tr}(\rho s_d) \\
&= \text{Tr}\left(\sum_{s'_d \in \tilde{\mathcal{P}}_n} \alpha_{s'_d} s'_d s_d\right) \\
&= \sum_{s'_d \in \tilde{\mathcal{P}}_n} \alpha_{s'_d} \text{Tr}(s'_d s_d) \\
&= \alpha_{s_d}.
\end{aligned} \tag{D20}$$

The fourth line uses

$$\text{Tr}(s_d s'_d) = \begin{cases} 0, & \text{if } s_d \neq s'_d, \\ 1, & \text{if } s_d = s'_d. \end{cases} \tag{D21}$$

Thus, α_{s_d} is obtained by evaluating $\text{Tr}(\rho s_d)$, where ρ is estimated via classical shadows. Using a set of POVMs (Positive Operator-Valued Measures) such as the random Pauli basis that measures each qubit and yields outcomes $|b\rangle \in \{0, 1\}^n$, the classical shadow is constructed as $\tilde{\rho} = \otimes_{j=1}^n \left(3P_j^\dagger |b_j\rangle \langle b_j| P_j - I\right)$, immediately gives $\alpha_{s_d} = \text{Tr}(\tilde{\rho} s_d)$.

b. Quantum State Tomography

Algorithm 1: Quantum State Learning Algorithm

-
- 1 **Input:** Data set $\mathcal{D}_{\text{QST}} = \{|\psi_j\rangle = \otimes_{i=1}^n |\psi_{j,i}\rangle\}_{j=1}^{N_{\text{data}}}$ and accuracy parameter ϵ .
 - 2 **Output:** $\hat{\rho}$ such that $\|\rho - \hat{\rho}\|_1 \leq \epsilon$.
 - 3 Let $l' = \lceil \log(1/\epsilon) \rceil$, enumerate all the legal $P \in \{I, X, Y, Z\}^{\otimes n}$ with $|P| \leq l'$.
 - 4 **For** $j \in [N_{\text{data}}]$:
 - 5 Using the SWAP-test to obtain the overlap v_j of ρ and $|\psi_j\rangle$.
 - 6 **End For**
 - 7 **For** each legal P :
 - 8 Compute $\alpha_P = \frac{3^{|P|}}{N_{\text{data}}} \sum_{j=1}^{N_{\text{data}}} v_j \langle \psi_j | P | \psi_j \rangle$,
 - 9 **End For**
 - 10 **Output:** $\hat{\rho} = \sum_{|P| \leq l'} \alpha_P P$
 - 11 **End**
-

This section is mainly about a way of learning α based on Ref.[86], which introduces a classical dataset to reconstruct the channel's output. Our results are given below.

Theorem 3 (Noisy Quantum State Learning, formal). *For any noisy quantum state ρ prepared by an unital noisy quantum circuit \mathcal{C} (Eq. B1), there exists a learning algorithm that can efficiently satisfy $\|\rho - \sum_{|P| \leq l'} \alpha_P P\|_1 \leq \epsilon$ with*

success probability $\geq 1 - \delta$. The learning algorithm requires sample complexity $N_{\text{data}} = 6^{\mathcal{O}\left(\frac{\log(1/\epsilon\delta)}{\log\left(\frac{4}{\sqrt[4]{15}}/(1-\gamma)^2\right)}\right)} \log(1/\delta)\epsilon^{-2}$ and classical post-processing complexity $n \cdot 24^{\mathcal{O}\left(\frac{\log(1/\epsilon\delta)}{\log\left(\frac{4}{\sqrt[4]{15}}/(1-\gamma)^2\right)}\right)} \log(1/\delta)\epsilon^{-2}$.

Details of our method are as follows.

Let Stab be a list of single-qubit stabilizers:

$$\text{Stab} = \{|0\rangle, |1\rangle, |+\rangle, |-\rangle, |y+\rangle, |y-\rangle\}. \quad (\text{D22})$$

Let $\{|\psi_j\rangle = \otimes_{i=1}^n |\psi_{i,j}\rangle\}_{j=1}^{N_{\text{data}}}$, where $|\psi_{i,j}\rangle \in \text{Stab}$.

$$\begin{aligned}
& \mathbb{E}_{|\psi_j\rangle \sim \text{Stab}^{\otimes n}} \langle \psi_j | \mathcal{C}(|0^n\rangle \langle 0^n|) |\psi_j\rangle \langle \psi_j | P | \psi_j \rangle \\
&= \sum_{|P| \leq l'} \alpha_P \mathbb{E}_{|\psi_j\rangle \sim \text{Stab}^{\otimes n}} \langle \psi_j | P | \psi_j \rangle \langle \psi_j | P | \psi_j \rangle \\
&= \sum_{|P| \leq l'} \alpha_P \mathbb{E}_{U \sim \text{Cl}(2)} \bigotimes_{i=1}^n \langle 0 | U_{i,j}^\dagger P U_{i,j} | 0 \rangle \langle 0 | U_{i,j}^\dagger P U_{i,j} | 0 \rangle \\
&= \frac{\alpha_P}{3^{|P|}} \bigotimes_{i=1}^n \sum_{Q_i \in \{X, Y, Z\}} \langle 0^2 | Q_i \otimes Q_i | 0^2 \rangle \\
&= \frac{\alpha_P}{3^{|P|}}.
\end{aligned} \quad (\text{D23})$$

The third line employs $|\psi_j\rangle = \otimes_{i=1}^n |\psi_{i,j}\rangle = \otimes_{i=1}^n U_{i,j} | 0 \rangle$, where $U_{i,j} \sim \text{Cl}(2)$. The fourth line uses

$$\mathbb{E}_{U_{i,j} \sim \text{Cl}(2)} \left[U_{i,j}^{\dagger \otimes 2} (Q_i \otimes Q_i) U_{i,j}^{\otimes 2} \right] = \begin{cases} I^{\otimes 2}, & \text{if } Q_i = Q_i' = I, \\ \frac{1}{3} \sum_{Q_i \in \{X, Y, Z\}^{\otimes 2}} (Q_i \otimes Q_i), & \text{if } Q_i = Q_i' \neq I, \\ 0, & \text{if } Q_i \neq Q_i'. \end{cases} \quad (\text{D24})$$

Therefore, α_P can be calculated by

$$\begin{aligned}
\alpha_P &= 3^{|P|} \mathbb{E}_{|\psi_j\rangle \sim \text{Stab}^{\otimes n}} \langle \psi_j | \rho | \psi_j \rangle \langle \psi_j | P | \psi_j \rangle \\
&\approx \frac{3^{|P|}}{N_{\text{data}}} \sum_{j=1}^{N_{\text{data}}} \langle \psi_j | \rho | \psi_j \rangle \langle \psi_j | P | \psi_j \rangle.
\end{aligned} \quad (\text{D25})$$

The first part of the summation term (of the form $\langle \psi_i | \rho | \psi_i \rangle$) can be obtained by using the SWAP-test method, while the latter part can be derived through classical post-processing. The data complexity N_{data} is $6^{\mathcal{O}(l')} \epsilon^{-2} \log(1/\delta)$, with failure probability δ . The proof follows a similar logic to that in Appendix E4, employing the triangle inequality and Hoeffding's inequality. The classical post-processing complexity is $\mathcal{O}(n \cdot N_{\text{data}} \cdot 2^{l'})$ according to the procedure presented in Algorithm 1 and Lemma 7.

Appendix E: Learning a Quantum Process Characterization

Compared with the noisy quantum state tomography, QPT is a more challenging task, which requires an exponential query complexity in the worst-case scenario Ref. [21], rendering it infeasible for large-scale systems. Inspired by the noisy quantum state tomography method, we proposed an efficient learning algorithm for the QPT task, particularly when the quantum process is given by a noisy quantum circuit \mathcal{C} (Eq. B1) followed by an unknown quantum measurement O . Without loss of generality, we assume the an n -qubit observable $O = \sum_{k=1}^M c_k Q_k$ with $M = \text{poly}(n)$, is the linear combinations of operators. Here, we do not restrict the locality of O , actually, it may include global Pauli terms with $|Q_k| = \mathcal{O}(n)$.

Let the noisy quantum channel be given by the Kraus decomposition $\mathcal{C} = \sum_j K_j(\cdot)K_j^\dagger$. It is observed that

$$\text{Tr}[\mathcal{C}(\rho_{\text{in}})O] = \text{Tr} \left[\sum_j K_j \rho_{\text{in}} K_j^\dagger O \right] = \text{Tr} \left[\sum_j \rho_{\text{in}} K_j^\dagger O K_j \right] = \text{Tr} [\rho_{\text{in}} \mathcal{C}^\dagger(O)]. \quad (\text{E1})$$

Consequently, the key step is to learn the 'dual' representation $\mathcal{C}^\dagger(O)$. We demonstrate that this dual operator also admits low-weight Pauli paths, allowing for a truncation-based approximation similar to that employed for noisy states.

1. Non-unital Noise

Ref. [77] gives a way of simulating arbitrary noise by Pauli propagation. Generally, a non-unital noise single-qubit channel \mathcal{E} can be decomposed as

$$\mathcal{E} = \mathcal{E}_{\text{depo}}^\gamma \circ \mathcal{E}', \quad (\text{E2})$$

where \mathcal{E}' is a suitable (non-physical) linear map and $\mathcal{E}_{\text{depo}}^\gamma$ is a depolarizing noise with the effective depolarizing rate $\gamma = 1 - \chi_{\mathcal{D}}(\mathcal{E})$:

$$\chi_{\mathcal{D}}^2(\mathcal{E}) := \max_{\mathcal{I} \subseteq [n]} \max_{\substack{\|O_{\mathcal{I}}\|_{\mathbb{F}} \neq 0 \\ \text{supp}(O_{\mathcal{I}}) = \mathcal{I}}} \left(\frac{\|\mathcal{E}^{\dagger \otimes n} O_{\mathcal{I}}\|_{\mathbb{F}}^2}{\|O_{\mathcal{I}}\|_{\mathbb{F}}^2} \right)^{1/|\mathcal{I}|} \quad (\text{E3})$$

is the mean squared contraction coefficient of \mathcal{E} in terms of the locally unbiased distribution \mathcal{D} . Given an observable $O = \sum_{P \in \mathcal{P}_n} \alpha_P P$, $O_{\mathcal{I}}$ retains those Pauli terms whose support is exactly \mathcal{I} : nontrivial on \mathcal{I} and identity elsewhere. $|\mathcal{I}|$ is the size of the $\text{supp}(O_{\mathcal{I}})$.

Channel \mathcal{E}' has the following property

$$\begin{aligned} \mathcal{E}'(I) &= \frac{\mathcal{E}(I)}{1-\gamma} - \frac{Ip}{1-\gamma}, \\ \mathcal{E}'(X) &= \frac{\mathcal{E}(X)}{1-\gamma}, \\ \mathcal{E}'(Y) &= \frac{\mathcal{E}(Y)}{1-\gamma}, \\ \mathcal{E}'(Z) &= \frac{\mathcal{E}(Z)}{1-\gamma}. \end{aligned} \quad (\text{E4})$$

Moreover, the adjoint channel \mathcal{E}'^\dagger satisfies

$$\begin{aligned}\mathcal{E}'^\dagger(I) &= I, \\ \mathcal{E}'^\dagger(X) &= \frac{\mathcal{E}^\dagger(X)}{1-\gamma}, \\ \mathcal{E}'^\dagger(Y) &= \frac{\mathcal{E}^\dagger(Y)}{1-\gamma}, \\ \mathcal{E}'^\dagger(Z) &= \frac{\mathcal{E}^\dagger(Z)}{1-\gamma}.\end{aligned}\tag{E5}$$

In that case, the output of noisy quantum circuits with non-unital channel can be written as

$$\begin{aligned}\mathcal{C}^\dagger(O) &= \sum_{s \in \tilde{\mathcal{P}}_n^{d+1}} s_0 \text{Tr}(s_1 \mathcal{C}_1^\dagger \mathcal{E}'^{\otimes n \dagger}(s_0)) \cdots \text{Tr}(s_d \mathcal{C}_d^\dagger \mathcal{E}'^{\otimes n \dagger}(s_{d-1})) \text{Tr}(s_d O) \\ &= \sum_{s \in \tilde{\mathcal{P}}_n^{d+1}} (1-\gamma)^{|s|} s_0 \Phi(\mathcal{C}^\dagger, s),\end{aligned}\tag{E6}$$

where $\Phi(\mathcal{C}^\dagger, s) = \text{Tr}(s_1 \mathcal{C}_1^\dagger \mathcal{E}'^{\otimes n \dagger}(s_0)) \cdots \text{Tr}(s_d \mathcal{C}_d^\dagger \mathcal{E}'^{\otimes n \dagger}(s_{d-1})) \text{Tr}(s_d O)$.

Lemma 3 (Contraction of the Non-unital adjoint map). *Let \mathcal{D} be a 1-design over $\text{SU}(2)$ and $\gamma = 1 - \chi_{\mathcal{D}}(\mathcal{E})$ be the effective depolarizing rate. For the (non-physical) linear map \mathcal{E}'^\dagger defined by its action on the Pauli basis $\{I/\sqrt{2}, X/\sqrt{2}, Y/\sqrt{2}, Z/\sqrt{2}\}$ as:*

$$\mathcal{E}'^\dagger(I/\sqrt{2}) = I/\sqrt{2}, \quad \mathcal{E}'^\dagger(\tilde{P}) = \frac{\mathcal{E}^\dagger(\tilde{P})}{1-\gamma} \quad \forall \tilde{P} \in \{X/\sqrt{2}, Y/\sqrt{2}, Z/\sqrt{2}\},\tag{E7}$$

the map is a contraction with respect to the Frobenius norm. That is, for any observable O , we have:

$$\|\mathcal{E}'^{\dagger \otimes n}(O)\|_2 \leq \|O\|_2,\tag{E8}$$

where $\|O\|_2 := \sqrt{\text{Tr}(O^\dagger O)}$ the Schatten 2-norm (or standard Frobenius norm).

Proof. Consider the Pauli decomposition of an arbitrary n -qubit observable $O = \sum_{\tilde{P} \in \tilde{\mathcal{P}}_n} \alpha_{\tilde{P}} \tilde{P}$, where $\tilde{\mathcal{P}}_n = \{I/\sqrt{2}, X/\sqrt{2}, Y/\sqrt{2}, Z/\sqrt{2}\}^{\otimes n}$ is the set of n -qubit Pauli strings. The Schatten 2-norm is given by $\|O\|_2^2 = \sum_{\tilde{P} \in \tilde{\mathcal{P}}_n} |\alpha_{\tilde{P}}|^2$.

By the definition of the mean squared contraction coefficient $\chi_{\mathcal{D}}(\mathcal{E})$, the scaling factor $1 - \gamma$ accounts for the maximum contraction of the adjoint noise channel \mathcal{E}^\dagger on the non-identity Pauli components. Specifically, for any $P \in \{X/\sqrt{2}, Y/\sqrt{2}, Z/\sqrt{2}\}$, the definition of γ implies $\|\mathcal{E}^\dagger(\tilde{P})\|_2 \leq 1 - \gamma$. Consequently, for the adjoint map, we have:

$$\|\mathcal{E}'^\dagger(\tilde{P})\|_2 = \frac{\|\mathcal{E}^\dagger(\tilde{P})\|_2}{1-\gamma} \leq 1.\tag{E9}$$

Since $\mathcal{E}'^\dagger(I/\sqrt{2}) = I/\sqrt{2}$, the norm of the identity component is preserved: $\|\mathcal{E}'^\dagger(I/\sqrt{2})\|_2 = 1$. Due to the orthogonality of the Pauli basis under the Hilbert-Schmidt inner product, the map acts independently on each Pauli component in the Frobenius sense:

$$\|\mathcal{E}'^{\dagger \otimes n}(O)\|_2^2 = \sum_{\tilde{P} \in \tilde{\mathcal{P}}_n} |\alpha_{\tilde{P}}|^2 \|\mathcal{E}'^{\dagger \otimes n}(\tilde{P})\|_2^2 \leq \sum_{\tilde{P} \in \tilde{\mathcal{P}}_n} |\alpha_{\tilde{P}}|^2 = \|O\|_2^2.\tag{E10}$$

This confirms that \mathcal{E}'^\dagger is a non-increasing map under the standard Frobenius norm, concluding the proof. \square

Definition 7 (Support-non-expanding). *A superoperator \mathcal{M} acting on the space of n -qubit operators is said to be support-non-expanding if, for any normalized Pauli string $\tilde{P} = \bigotimes_{i=1}^n \tilde{P}_i \in \tilde{\mathcal{P}}_n$, the image $\mathcal{M}(\tilde{P})$ can be decomposed as a linear combination of normalized Pauli strings $\{\tilde{Q}^{(k)}\}$ such that for each k with a non-zero coefficient, the support of $\tilde{Q}^{(k)}$ is a subset of the support of \tilde{P} :*

$$\text{supp}(\tilde{Q}^{(k)}) \subseteq \text{supp}(\tilde{P}), \quad \forall k.\tag{E11}$$

Alternatively, if $\mathcal{M} = \bigotimes_{i=1}^n \mathcal{M}_i$ is a tensor product of single-qubit maps, it is support-non-expanding if each \mathcal{M}_i satisfies $\mathcal{M}_i(\tilde{P}_i) \in \text{span}\{I/\sqrt{2}, X/\sqrt{2}, Y/\sqrt{2}, Z/\sqrt{2}\}$ for any non-identity \tilde{P}_i , and specifically:

$$\mathcal{M}_i(\tilde{I}) \propto \tilde{I}, \quad (\text{E12})$$

where $\tilde{I} = I/\sqrt{2}$ is the normalized single-qubit identity operator.

2. Quantum Process Approximation

Lemma 4 (Unified Noisy Process Truncation). *Let \mathcal{C} be a d -depth noisy quantum circuit composed of two-qubit Haar random gates and i.i.d. single-qubit noisy channels \mathcal{E} with noise strength γ . With probability $\geq 1 - \delta_2$, for any arbitrary input ρ_{in} , there exists a truncated operator $\mathcal{C}^{(l')\dagger}(O)$ with Pauli weight at most l' such that the approximation error is bounded by ϵ_2 . The required truncation degree l' scales logarithmically with the target precision and inversely with the effective decay rate:*

$$l' = \mathcal{O}\left(\frac{\log(\|O\|_{\mathbb{F}}^2/\epsilon_2^2\delta_2)}{\log(\Lambda(1-\gamma)^{-2})}\right). \quad (\text{E13})$$

Here, the error metric and the structural scrambling constant Λ depend on the noise type:

- **Unital Noise:** The error is bounded in the operator norm $\left|\text{Tr}\left[\rho_{\text{in}}(\mathcal{C}^{(l')\dagger}(O) - \mathcal{C}^\dagger(O))\right]\right| \leq \epsilon_2$, with $\Lambda = \sqrt[4]{15}$.
- **Non-unital Noise:** The error is bounded in the operator norm $\left|\text{Tr}\left[\rho_{\text{in}}(\mathcal{C}^{(l')\dagger}(O) - \mathcal{C}^\dagger(O))\right]\right| \leq \epsilon_2$, with $\Lambda \approx \sqrt{15}$ (neglecting second-order terms $\mathcal{O}(\gamma^2)$).

We prove it by proof the unital noise and the non-unital noise respectively.

Given $O = \sum_{P \in \mathcal{P}_n} \alpha_P P$, the noisy process characterization can be represented by

$$\mathcal{C}^\dagger(O) = \sum_{s \in \tilde{\mathcal{P}}_n^{d+1}} (1-\gamma)^{|s|} \Phi(\mathcal{C}^\dagger, s) s_0, \quad (\text{E14})$$

where

$$\Phi(\mathcal{C}^\dagger, s) = \begin{cases} \text{Tr}(s_1 \mathcal{C}_1^\dagger(s_0)) \cdots \text{Tr}(s_d \mathcal{C}_d^\dagger(s_{d-1})) \text{Tr}(s_d O), & \text{unital,} \\ \text{Tr}(s_1 \mathcal{C}_1^\dagger \mathcal{E}'^{\otimes n \dagger}(s_0)) \cdots \text{Tr}(s_d \mathcal{C}_d^\dagger \mathcal{E}'^{\otimes n \dagger}(s_{d-1})) \text{Tr}(s_d O), & \text{non-unital.} \end{cases} \quad (\text{E15})$$

Lemma 5 (The unital noisy process truncation). *Let the noisy quantum circuit $\mathcal{C} = \mathcal{E}^{\otimes n} \mathcal{C}_d \mathcal{E}^{\otimes n} \mathcal{C}_{d-1} \cdots \mathcal{E}^{\otimes n} \mathcal{C}_1$ represent a d -depth noisy quantum circuit, where \mathcal{C}_i is a layer of two-qubit Haar random quantum gates and \mathcal{E} represents an i.i.d unital single-qubit noisy channel with noise strength γ . With nearly unit success probability $\geq 1 - \delta_2$, for any arbitrary input ρ_{in} , there exists an operator $\mathcal{C}^{(l')\dagger}(O) = \sum_{|\tilde{P}| \leq l', \tilde{P} \in \tilde{\mathcal{P}}_n} \beta_{\tilde{P}} P$ such that*

$$\left|\text{Tr}\left[\rho_{\text{in}}(\mathcal{C}^{(l')\dagger}(O) - \mathcal{C}^\dagger(O))\right]\right| \leq \epsilon_2, \quad (\text{E16})$$

where the coefficients $\beta_{\tilde{P}} \in \mathbb{R}$ are the Pauli expansion coefficients of the evolved operator, and $l' = \mathcal{O}\left(\frac{\log(\|O\|_{\mathbb{F}}^2/\epsilon_2^2\delta_2)}{\log(\sqrt[4]{15}/(1-\gamma)^2)}\right)$.

Proof. Considering the unital noise, let

$$\begin{aligned} \mathbb{E}_{\mathcal{C}}(\Delta^2) &:= \mathbb{E}_{\mathcal{C}} \left| \text{Tr}\left[\rho_{\text{in}}(\mathcal{C}^{(l')\dagger}(O) - \mathcal{C}^\dagger(O))\right] \right|^2 \\ &= \mathbb{E}_{\mathcal{C}} \left| \text{Tr}\left[\rho_{\text{in}} \sum_{|\tilde{P}| > l', \tilde{P} \in \tilde{\mathcal{P}}_n} \beta_{\tilde{P}} \tilde{P}\right] \right|_2^2 \\ &= \mathbb{E}_{\mathcal{C}} \left(\sum_{|s| > l} (1-\gamma)^{2|s|} \Phi(\mathcal{C}, s)^2 \text{Tr}(s_0 \rho_{\text{in}})^2 \right) \\ &= \sum_{k > l} (1-\gamma)^{2k} V_k, \end{aligned} \quad (\text{E17})$$

where we define V_k as

$$\begin{aligned}
V_k &:= \mathbb{E}_{\mathcal{C}, |s|=k} \text{Tr}(s_0 \rho_{\text{in}})^2 \Phi(\mathcal{C}^\dagger, s)^2 \\
&= \mathbb{E}_{\mathcal{C}, |s|=k} \left(\text{Tr}(s_0 \rho_{\text{in}}) \text{Tr}(s_1 \mathcal{C}_1^\dagger(s_0)) \cdots \text{Tr}(s_d \mathcal{C}_d^\dagger(s_{d-1})) \text{Tr}(s_d O) \right)^2 \\
&\leq \alpha_{\tilde{s}_d}^2 \mathbb{E}_{\mathcal{C}_1} (\text{Tr}(s_1 \mathcal{C}_1^\dagger(s_0)))^2 \cdots \mathbb{E}_{\mathcal{C}_d} (\text{Tr}(s_d \mathcal{C}_d^\dagger(s_{d-1})))^2 \\
&\leq \alpha_{\tilde{s}_d}^2 \left(\frac{1}{15} \right)^{\frac{k}{4}}.
\end{aligned} \tag{E18}$$

Here, the operator $\tilde{s}_d = 2^{n/2} s_d$ represents the standard Pauli operator, and the related coefficient satisfies $\alpha_{\tilde{s}_d} = 2^{-n/2} \alpha_{s_d}$. As a result, we can upper bound

$$\begin{aligned}
\mathbb{E}(\Delta^2) &\leq \sum_{k>l} (1-\gamma)^{2k} \alpha_{\tilde{s}_d}^2 \left(\frac{1}{15} \right)^{\frac{k}{4}} \\
&\leq (1-\gamma)^{2l} \left(\frac{1}{15} \right)^{\frac{l}{4}} \sum_{k>l} \alpha_{\tilde{s}_d}^2 \\
&\leq (1-\gamma)^{2l} \left(\frac{1}{15} \right)^{\frac{l}{4}} \|O\|_{\mathbb{F}}^2.
\end{aligned} \tag{E19}$$

By Markov inequality when $l' = \mathcal{O}(l) = \mathcal{O}\left(\frac{\log(\|O\|_{\mathbb{F}}^2/\epsilon_2^2 \delta_2)}{\log(\frac{1}{\sqrt{15}}/(1-\gamma)^2)}\right)$, $\Delta \leq \epsilon_2$ is satisfied with the success probability $\geq 1 - \delta_2$. \square

Here we use this property Eq. E5 to prove that the truncation works without the requirement of the non-unital noise strength, which is

Lemma 6 (The non-unital noisy process truncation). *Let the noisy quantum circuit $\mathcal{C} = \mathcal{E}^{\otimes n} \mathcal{C}_d \mathcal{E}^{\otimes n} \mathcal{C}_{d-1} \cdots \mathcal{E}^{\otimes n} \mathcal{C}_1$ represent a d -depth noisy quantum circuit, where \mathcal{C}_i is a layer of two-qubit Haar random quantum gates and \mathcal{E} represents an i.i.d non-unital single-qubit noisy channel with noise strength γ . With nearly unit success probability $\geq 1 - \delta_2$, there exists an operator $\mathcal{C}^{(l')\dagger}(O) = \sum_{|\tilde{P} \leq l', \tilde{P} \in \tilde{\mathcal{P}}_n} \beta_{\tilde{P}} \tilde{P}$ such that*

$$\left| \text{Tr} \left[\rho_{\text{in}} (\mathcal{C}^{(l')\dagger}(O) - \mathcal{C}^\dagger(O)) \right] \right| \leq \epsilon_2, \tag{E20}$$

where coefficients $\beta_{\tilde{P}} \in \mathbb{R}$ and $l' = \frac{\log(\|O\|_{\mathbb{F}}^2/(\epsilon_2^2 \delta_2))}{\log(1/[(1-\gamma)^2(\frac{1}{\sqrt{15}} + \mathcal{O}(\gamma^2))])}$.

Proof. For each term in the form of $\text{Tr}(s_j \mathcal{C}_j^\dagger \mathcal{E}'^{\otimes n \dagger}(s_{j-1}))$, we have

$$\begin{aligned}
\mathbb{E}_{\mathcal{C}_j} [\text{Tr}[s_j \mathcal{C}_j^\dagger \mathcal{E}'^{\otimes n \dagger}(s_{j-1})]^2] &= \mathbb{E}_{\mathcal{C}_j} [\text{Tr}[\mathcal{E}'^{\otimes n \dagger}(s_{j-1}) \mathcal{C}_j s_j \mathcal{C}_j^\dagger]^2] \\
&= \mathbb{E}_{\mathcal{C}_j} [\text{Tr}[\mathcal{E}'^{\otimes n \dagger}(s_{j-1}) \mathcal{C}_j(s_j)]^2] \\
&\leq \left(\frac{1}{15} \right)^{|\mathcal{E}'^{\otimes n \dagger}(s_{j-1})/2|} \|\mathcal{E}'^{\otimes n \dagger}(s_{j-1})\|_2^2 \\
&\leq \left(\frac{1}{15} \right)^{|\mathcal{E}'^{\otimes n \dagger}(s_{j-1})/2|} \|s_{j-1}\|_2^2 \\
&\leq \left(\frac{1}{15} \right)^{|\mathcal{E}'^{\otimes n \dagger}(s_{j-1})/2|}.
\end{aligned} \tag{E21}$$

The Third line is from Eq. D15. The Fourth line is due to the property of the Eq. E5 and Lemma 3, which conveys that \mathcal{E}'^\dagger does not increase the standard Frobenius norm of Pauli strings.

Consider the adjoint map \mathcal{E}'^\dagger acting on a single-qubit Pauli operator $\tilde{P} \in \{X/\sqrt{2}, Y/\sqrt{2}, Z/\sqrt{2}\}$. For any local CPTP noise channel (including non-unital ones like amplitude damping), the action can be decomposed into a Pauli-preserving part and an identity-generating part:

$$\mathcal{E}'^\dagger(\tilde{P}) = b_{\tilde{P}} \tilde{P} + b_I \frac{I}{\sqrt{2}} + \sum_{\tilde{Q} \in \{X/\sqrt{2}, Y/\sqrt{2}, Z/\sqrt{2}\}, \tilde{Q} \neq \tilde{P}} b_{\tilde{Q}} \tilde{Q}, \tag{E22}$$

where $b_{\tilde{P}}, b_I, b_{\tilde{Q}}$ are the corresponding expansion coefficients. According to Lemma 3, the map \mathcal{E}^\dagger is Frobenius-contractive, which implies the following normalization constraint on these coefficients:

$$|b_{\tilde{P}}|^2 + |b_I|^2 + \sum_{\tilde{Q} \neq \tilde{P}} |b_{\tilde{Q}}|^2 = \|\mathcal{E}^\dagger(\tilde{P})\|_2^2 \leq 1. \quad (\text{E23})$$

When this operator is evolved through a 2-design unitary layer \mathcal{C}_j , we evaluate the expected contribution of the Pauli path. For a normalized Pauli string s_{j-1} , the map $\mathcal{E}^{\dagger \otimes n}$ produces a superposition of Pauli strings:

$$\mathcal{E}^{\dagger \otimes n}(s_{j-1}) = \sum_{w \subseteq \text{supp}(s_{j-1})} B_w w, \quad (\text{E24})$$

where B_w are product coefficients of the single-qubit terms. Note that the map is support-non-expanding, ensuring the Hamming weight of any component $|w| \leq |s_{j-1}|$.

To strictly bound the expectation using the fixed input weight $|s_{j-1}|$ rather than the variable output weight $|w|$, we exploit the independence of the noise channel on each qubit.

Since the full adjoint map $\mathcal{E}^{\dagger \otimes n}$ is a tensor product of identical single-qubit maps \mathcal{E}^\dagger , the sum over all generated Pauli strings w factorizes into a product over the individual active qubits in the support of s_{j-1} .

For each active qubit $i \in \text{supp}(s_{j-1})$, the single-qubit map \mathcal{E}^\dagger produces:

- An identity component $I/\sqrt{2}$ (weight 0) with coefficient $|b_I|^2$. We denote this non-unital leakage strength as $\nu = |b_I|^2$.
- A Pauli component $\tilde{P} \in \{X/\sqrt{2}, Y/\sqrt{2}, Z/\sqrt{2}\}$ (weight 1) with total probability mass $\sum_{\tilde{Q}} |b_{\tilde{Q}}|^2 \leq 1 - \nu$.

Substituting the operator decomposition into the expectation over the 2-design layer \mathcal{C}_j , the global sum exactly decomposes into a product of local expectations due to the tensor-product structure of the noise and the layer:

$$\begin{aligned} \mathbb{E}_{\mathcal{C}_j}[\text{Tr}(\mathcal{E}^{\dagger \otimes n}(s_{j-1})\mathcal{C}_j(s_j))^2] &= \sum_{w \subseteq s_{j-1}} |B_w|^2 \left(\frac{1}{15}\right)^{|w|/2} \\ &= \prod_{i \in \text{supp}(s_{j-1})} \left(\underbrace{\left(\sum_{\tilde{Q}} |b_{\tilde{Q}}|^2\right)}_{\text{stay Pauli}} \frac{1}{\sqrt{15}} + \underbrace{|b_I|^2}_{\text{become } I} \cdot 1 \right). \end{aligned} \quad (\text{E25})$$

Let $\nu = |b_I|^2$ denote the leakage probability to the identity. Using the normalization condition $\sum_{\tilde{Q}} |b_{\tilde{Q}}|^2 \leq 1 - \nu$, the term inside the product for each qubit is bounded by:

$$\mu(\nu) := (1 - \nu) \frac{1}{\sqrt{15}} + \nu = \frac{1}{\sqrt{15}} + \nu \left(1 - \frac{1}{\sqrt{15}}\right). \quad (\text{E26})$$

For standard physical noise models such as amplitude damping with rate γ , a direct expansion of the Kraus operators verifies that the identity coefficient scales linearly with the noise rate, i.e., $b_I \propto \gamma$. Consequently, the leakage strength scales quadratically as $\nu = |b_I|^2 = \mathcal{O}(\gamma^2)$.

Substituting this scaling back into the product over the $|s_{j-1}|$ active qubits, we obtain the total suppression factor for the layer:

$$\begin{aligned} \mathbb{E}_{\mathcal{C}_j}[\text{Tr}(\mathcal{E}^{\dagger \otimes n}(s_{j-1})\mathcal{C}_j(s_j))^2] &= \prod_{i \in \text{supp}(s_{j-1})} \mu(\nu) \\ &\leq \left(\frac{1}{\sqrt{15}} + \mathcal{O}(\gamma^2)\right)^{|s_{j-1}|}. \end{aligned} \quad (\text{E27})$$

This confirms that the suppression is dominated by the structural scrambling constant $1/\sqrt{15}$, with only a second-order perturbation from the noise.

This rigorous factorization allows us to establish the recursive relation without ambiguity regarding the variable weights.

We first analyze the variance contribution W_k of Pauli paths with output weight k . To rigorously bound the expectation, we utilize the independence of the noise channels. Since the adjoint map $\mathcal{E}^{\dagger \otimes n}$ is a tensor product of

single-qubit maps, the expectation over a 2-design layer \mathcal{C}_j factorizes into a product over the active qubits in the support of s_{j-1} . For each active qubit, the map produces an identity component I with coefficient $\nu = |b_I|^2$, and a Pauli component with mass at most $1 - \nu$.

Substituting this into the expectation, the suppression factor for the j -th layer is bounded by:

$$\begin{aligned} \mathbb{E}_{\mathcal{C}_j}[\text{Tr}(\mathcal{E}'^{\dagger \otimes n}(s_{j-1})\mathcal{C}_j(s_j))^2] &= \prod_{i \in \text{supp}(s_{j-1})} \left((1 - \nu) \left(\frac{1}{15} \right)^{1/2} + \nu \cdot 1 \right) \\ &= \left(\frac{1}{\sqrt{15}} + \nu \left(1 - \frac{1}{\sqrt{15}} \right) \right)^{|s_{j-1}|}. \end{aligned} \quad (\text{E28})$$

This indicates that the structural suppression rate is strictly determined by the weight of the input string. Now, we bound W_k . Recall that W_k is defined as the expectation of the sum over all paths ending with weight k . By linearity of expectation, we can interchange the expectation and the summation:

$$\begin{aligned} V_k &= \mathbb{E}_{\mathcal{C}, |s|=k} \text{Tr}(s_0 \rho_{\text{in}})^2 \Phi(\mathcal{C}^\dagger, s)^2 \\ &= \mathbb{E}_{\mathcal{C}, |s|=k} \left(\text{Tr}(s_0 \rho_{\text{in}}) \text{Tr}(s_1 \mathcal{C}_1^\dagger \mathcal{E}'^{\otimes n \dagger}(s_0)) \cdots \text{Tr}(s_d \mathcal{C}_d^\dagger \mathcal{E}'^{\otimes n \dagger}(s_{d-1})) \text{Tr}(s_d O) \right)^2 \\ &\leq \alpha_{s_d}^2 \mathbb{E}_{\mathcal{C}} \left(\text{Tr}(s_1 \mathcal{C}_1^\dagger \mathcal{E}'^{\otimes n \dagger}(s_0)) \cdots \text{Tr}(s_d \mathcal{C}_d^\dagger \mathcal{E}'^{\otimes n \dagger}(s_{d-1})) \right) \\ &\leq \alpha_{s_d}^2 \left(\frac{1}{\sqrt{15}} + \mathcal{O}(\gamma^2) \right)^k. \end{aligned} \quad (\text{E29})$$

The total truncation error $\mathbb{E}[\Delta^2]$ sums the contributions from all Pauli strings with weight $|s| > l$. Incorporating the physical noise decay factor $(1 - \gamma)^2$ per layer from the forward process, the total error is bounded by a geometric series:

$$\begin{aligned} \mathbb{E}[\Delta^2] &= \mathbb{E}_{\mathcal{C}} \sum_{|s| > l} (1 - \gamma)^{2|s|} \text{Tr}(s_0 \rho_{\text{in}})^2 \Phi(\mathcal{C}^\dagger, s)^2 \\ &\leq (1 - \gamma)^{2l} \sum_{k > l} V_k \\ &\leq (1 - \gamma)^{2l} \sum_{k > l} \alpha_{s_d}^2 \left(\frac{1}{\sqrt{15}} + \mathcal{O}(\gamma^2) \right)^k \\ &\leq (1 - \gamma)^{2l} \left(\frac{1}{\sqrt{15}} + \mathcal{O}(\gamma^2) \right)^l \sum_{k > l} \alpha_{s_d}^2 \\ &= \|O\|_{\mathbb{F}}^2 \left[(1 - \gamma)^2 \left(\frac{1}{\sqrt{15}} + \mathcal{O}(\gamma^2) \right) \right]^{l'}. \end{aligned} \quad (\text{E30})$$

Let R be the combined decay ratio given by:

$$R(\gamma, \nu) = (1 - \gamma)^2 \left[(1 - \nu) \frac{1}{\sqrt{15}} + \nu \right]. \quad (\text{E31})$$

Since $\nu \in [0, 1)$ for any physical noise $\gamma < 1$, the term in brackets is a convex combination of $1/\sqrt{15}$ and 1. We bound it strictly by the maximum of its components:

$$(1 - \nu) \frac{1}{\sqrt{15}} + \nu \cdot 1 < 1. \quad (\text{E32})$$

Substituting this structural bound back into R :

$$R(\gamma, \nu) < (1 - \gamma)^2 \cdot 1 = (1 - \gamma)^2. \quad (\text{E33})$$

Now we analyze the convergence condition $R < 1$ for the entire physical regime $\gamma \in [0, 1)$:

- **Case 1: Noisy Regime** ($\gamma \in (0, 1)$). The physical decay is strictly contractive, i.e., $(1 - \gamma)^2 < 1$. Thus, $R \leq (1 - \gamma)^2 < 1$.

- **Case 2: Noiseless Limit** ($\gamma = 0$). In this limit, leakage vanishes ($\nu = 0$). The ratio reduces to the pure structural suppression $R = 1/\sqrt{15} < 1$.

Combining both cases, we have $R < 1$ for all $\gamma \in [0, 1)$. This strictly ensures the convergence of the geometric series. The summation yields:

$$\mathbb{E}[\Delta^2] \leq \|O\|_{\mathbb{F}}^2 R^{l'}. \quad (\text{E34})$$

The last proof is similar to the Appendix D 2. Therefore when

$$l' = \mathcal{O}(l) = \frac{\log(\|O\|_{\mathbb{F}}^2/(\epsilon_2^2 \delta_2))}{\log(1/R)} = \frac{\log(\|O\|_{\mathbb{F}}^2/(\epsilon_2^2 \delta_2))}{\log\left(1/\left[(1-\gamma)^2\left(\frac{1}{\sqrt{15}} + \mathcal{O}(\gamma^2)\right)\right]\right)}, \quad (\text{E35})$$

$\Delta \leq \epsilon_2$ is satisfied with the success probability $\geq 1 - \delta_2$. □

3. Algorithm of process learning

Similar to the noisy quantum state tomography task, reconstructing $\mathcal{C}^{(l')\dagger}(O)$ proceeds from the data set $\mathcal{D}_{\text{QPT}} = \{|\psi_j\rangle = \otimes_{i=1}^n |\psi_{i,j}\rangle, \phi_j = \text{Tr}[OC(|\psi_j\rangle\langle\psi_j|)]\}_{j=1}^{N_{\text{data}}}$, where $|\psi_{i,j}\rangle$ is a single-qubit stabilizer randomly sampled from the set Stab , and ϕ_j denotes the output of the target quantum process. According to the Eq. D24, coefficients β_P can be learned efficiently via

$$\beta_P = \frac{3^{|P|}}{N_{\text{data}}} \sum_{i=1}^{N_{\text{data}}} \phi_j \langle\psi_i| P |\psi_i\rangle. \quad (\text{E36})$$

The complete QPT procedure is summarized in Algorithm 2.

Algorithm 2: Quantum Process Learning Algorithm

- 1 **Input:** Data set $\mathcal{D}_{\text{QPT}} = \{|\psi_j\rangle = \otimes_{i=1}^n |\psi_{i,j}\rangle\}_{j=1}^{N_{\text{data}}}$ and accuracy parameter ϵ ;
 - 2 **Output:** A $f(\cdot)$ such that $|f(\cdot) - \text{Tr}[OC(\cdot)]| \leq \epsilon$ with high success probability for all input quantum states;
 - 3 Let $l' = \lceil \log(1/\epsilon) \rceil$, enumerate all the $P \in \mathcal{P}_n$ with $|P| \leq l'$;
 - 4 **For** $j \in [N_{\text{data}}]$:
 - 5 Take the input state $|\psi_j\rangle\langle\psi_j|$ into the target quantum process, and obtain the output $\phi_j = \text{Tr}[OC(|\psi_j\rangle\langle\psi_j|)]$;
 - 6 **End For**
 - 7 **For** each $P \in \mathcal{P}_n$ with $|P| \leq l'$:
 - 8 Compute $\beta_P = \frac{3^{|P|}}{N_{\text{data}}} \sum_{j=1}^{N_{\text{data}}} \phi_j \langle\psi_j| P |\psi_j\rangle$.
 - 9 **End For**
 - 10 **Output:** $f(\cdot) = \sum_{|P| \leq l'} \beta_P \text{Tr}(P(\cdot))$
-

4. proof of Theorem 2

In this section, we will prove the main result of our learning algorithm.

Theorem 4 (Noisy Quantum Process Learning, formal). *For any noisy quantum process \mathcal{C} defined as Eq. B1, where C_i is a layer of two-qubit Haar random quantum gates, and an n -qubit observable $O = \sum_{k=1}^M c_k Q_k$ with $M = \text{poly}(n)$, there exists a learning algorithm f , such that for any $\epsilon \in (0, 1)$ and input quantum state ρ_{in} , $|f(\rho_{\text{in}}) - \text{Tr}(OC(\rho_{\text{in}}))| < \epsilon$ with success probability $\geq 1 - \delta$. The learning algorithm requires sample complexity*

$$N_{\text{data}} = 6 \left(\frac{\log(\|O\|_{\mathbb{F}}^2/(\epsilon\delta))}{\log\left(1/\left[(1-\gamma)^2\left(15^{-1/2} + \mathcal{O}(\gamma^2)\right)\right]\right)} \right) \log(\delta^{-1}) \epsilon^{-2}, \quad (\text{E37})$$

and classical post-processing complexity $\mathcal{O}\left(n \cdot 24 \left(\frac{\log(\|O\|_{\mathbb{F}}^2/(\epsilon\delta))}{\log\left(1/\left[(1-\gamma)^2\left(15^{-1/2} + \mathcal{O}(\gamma^2)\right)\right]\right)} \right) \log(\delta^{-1}) \epsilon^{-2}\right)$.

Moreover, if the noise is unital, the sample complexity is $6^{\mathcal{O}\left(\frac{\log(\|O\|_{\mathbb{F}}/\epsilon_2^2\delta_2)}{\log(\sqrt[4]{15}/(1-\gamma)^2)}\right)} \log(\delta^{-1})\epsilon^{-2}$ and classical post-processing complexity is $\mathcal{O}\left(n \cdot 24^{\mathcal{O}\left(\frac{\log(\|O\|_{\mathbb{F}}/\epsilon_2^2\delta_2)}{\log(\sqrt[4]{15}/(1-\gamma)^2)}\right)} \log(\delta^{-1})\epsilon^{-2}\right)$.

Proof. The discrepancy between the algorithm's learned outcome and the true value, quantified via absolute value, encompasses two types of errors: truncation error and learning error.

$$\begin{aligned} |f(\rho_{\text{in}}) - \text{Tr}(\mathcal{C}(\rho_{\text{in}})O)| &= \left| \sum_{|P|\leq l'} \hat{\beta}_P \text{Tr}(\rho_{\text{in}}P) - \text{Tr}(\mathcal{C}(\rho_{\text{in}})O) \right| \\ &\leq \left| \sum_{|P|\leq l'} \beta_P \text{Tr}(\rho_{\text{in}}P) - \text{Tr}(\mathcal{C}(\rho_{\text{in}})O) \right| + \left| \sum_{|P|\leq l'} \hat{\beta}_P \text{Tr}(\rho_{\text{in}}P) - \sum_{|P|\leq l'} \beta_P \text{Tr}(\rho_{\text{in}}P) \right| \\ &= \left| \sum_{|\tilde{P}|\leq l'} \beta_{\tilde{P}} \text{Tr}(\rho_{\text{in}}\tilde{P}) - \text{Tr}(\mathcal{C}(\rho_{\text{in}})O) \right| + \left| \sum_{|P|\leq l'} \hat{\beta}_P \text{Tr}(\rho_{\text{in}}P) - \sum_{|P|\leq l'} \beta_P \text{Tr}(\rho_{\text{in}}P) \right|. \end{aligned} \quad (\text{E38})$$

The inequality is derived through the application of the triangle inequality, where the first term on the right-hand side of the inequality represents the truncation error, and the second term represents the learning error. $\hat{\beta}_P$ denotes the learned value of β_P .

The proof for the truncation error can be analogously extended from that in Appendix E2, demonstrating that when $l' = \mathcal{O}\left(\frac{\log(\|O\|_{\mathbb{F}}^2/\epsilon_2^2\delta_2)}{\log(\Lambda(1-\gamma)^{-2})}\right)$, $\left| \sum_{|P|\leq l'} \beta_P \text{Tr}(\rho_x P) - \text{Tr}(\mathcal{C}(\rho_x)O) \right| \leq \epsilon_2$.

The learning error is bounded by

$$\begin{aligned} \left| \left(\sum_{|P|\leq l'} \hat{\beta}_P - \sum_{|P|\leq l'} \beta_P \right) \text{Tr}(\rho_{\text{in}}P) \right| &\leq \left| \sum_{|P|\leq l'} \hat{\beta}_P - \sum_{|P|\leq l'} \beta_P \right| \\ &= \sum_{|P|\leq l'} |\hat{\beta}_P - \beta_P| \\ &\leq N_s |\hat{\beta}_P - \beta_P| \\ &\leq \epsilon_3. \end{aligned} \quad (\text{E39})$$

Combining the equation with Hoeffding's inequality, we can derive that given a dataset of size $N_{\text{data}} = \frac{3^{\mathcal{O}(l')N_s}}{\epsilon_3^2} \log \frac{1}{\delta}$ with probability at least $1 - \delta$, Eq. E39 is valid.

Lemma 7 (Number of the Legal Pauli Paths). *For any noisy quantum process \mathcal{C} defined as Eq. B1, the number of the legal Pauli paths, denoted as N_s is $2^{\mathcal{O}(l')}$ for our QST and QPT task.*

The proof of Lemma 7 is provided in the next section. Considering Lemma 7, for an arbitrary i.i.d single-qubit noise, given $\epsilon_2 = \epsilon_3$, the sample complexity can be further expressed as

$$N_{\text{data}} = 6^{\mathcal{O}(\log(\|O\|_{\mathbb{F}}^2/\epsilon_2^2\delta_2)/\log(\Lambda(1-\gamma)^{-2}))} \log(\delta^{-1})\epsilon^{-2}. \quad (\text{E40})$$

For the runtime complexity of classical post-processing, the calculation is derived directly from Algorithm 2. The dominant factor in the runtime is the computation of the coefficients β_P , which involves nested iterations over N_{data} input samples and N_s Pauli strings. The internal calculation of the expectation value $\langle \psi_j | P | \psi_j \rangle$ has a cost of $\mathcal{O}(n)$, because the input state $|\psi_j\rangle$ is a product state and P is a Pauli string, allowing the expectation value to be computed via the product of n single-qubit terms.

Thus, the total complexity is:

$$\mathcal{O}(n \cdot N_{\text{data}} \cdot N_s) = \mathcal{O}\left(n \cdot 24^{\mathcal{O}(\log(\|O\|_{\mathbb{F}}^2/\epsilon_2^2\delta_2)/\log(\Lambda(1-\gamma)^{-2}))} \log(\delta^{-1})\epsilon^{-2}\right), \quad (\text{E41})$$

where the factor n accounts for the linear cost of evaluating the n single-qubit terms that constitute $\langle \psi_j | P | \psi_j \rangle$ for each pair of sample $|\psi_j\rangle$ and Pauli string P .

Under the condition that $\Lambda > 1$, the sample complexity and runtime complexity scale as $\text{poly}(n, 1/\epsilon)$ for any noise strength γ . □

5. Number of the legal Pauli paths

Regarding the number of legal Pauli paths, denoted by N_s , we observe that for $l \geq d + 1$, the weight L_k that

$$L_k = \begin{cases} \mathbb{E}_{\mathcal{C}, |s|=k} (\text{Tr}(s_d \mathcal{C}_d(s_{d-1})) \cdots \text{Tr}(s_1 \mathcal{C}_1(s_0)))^2 & \text{unital QST} \\ \mathbb{E}_{\mathcal{C}, |s|=k} (\text{Tr}(s_1 \mathcal{C}_1^\dagger(s_0)) \cdots \text{Tr}(s_d \mathcal{C}_d^\dagger(s_{d-1})))^2 & \text{unital QPT} \\ \mathbb{E}_{\mathcal{C}, |s|=k} (\text{Tr}(s_1 \mathcal{C}_1^\dagger \mathcal{E}'^{\otimes n \dagger}(s_0)) \cdots \text{Tr}(s_d \mathcal{C}_d^\dagger \mathcal{E}'^{\otimes n \dagger}(s_{d-1})))^2 & \text{non-unital QPT} \end{cases} \quad (\text{E42})$$

admits a lower bound of $L_k \geq (1/15)^k$. Crucially, this bound holds even for non-unital noise, owing to the property $|\mathcal{E}'^\dagger(\tilde{P})| \leq |\tilde{P}|$.

By Eqs. D15 and E28, L_k follows a convergent geometric progression with respect to k , ensuring that $\sum_{k=d+1}^l L_k = \mathcal{O}(1)$. Furthermore,

$$\begin{aligned} \mathcal{O}(1) &= \sum_{k=d+1}^l L_k + L_0 \\ &\geq \sum_{k=d+1}^l \left(\frac{1}{15}\right)^k + 1 \\ &\geq \sum_{k=d+1}^l \left(\frac{1}{15}\right)^l + 1 \\ &= \left(\frac{1}{15}\right)^l N_{|s| \in [d+1, l]} + 1. \end{aligned} \quad (\text{E43})$$

where $N_{|s| \in [d+1, l]}$ denotes the legal Pauli paths except all identity one. The number of Pauli paths needed is

$$N_s = N_{|s| \in [d+1, l]} + 1 = \mathcal{O}(1)15^l = 2^{\mathcal{O}(l)} = 2^{\mathcal{O}(l')}. \quad (\text{E44})$$

In our learning framework, we focus on the terminal Pauli operators s_d rather than the internal path trajectories. Since the collective influence of all contributing paths is implicitly encapsulated within the learned coefficients $\{\beta_P\}$, the complexity is governed by the Hamming weight of the output operators, l' . To establish the relationship between l and l' , we note that any non-trivial Pauli path must account for at least one non-identity operation per layer to remain active during the d -layer evolution, yielding $L_k = 0$ for $1 \leq k \leq d$. This implies that for a total path weight l , the remaining degrees of freedom for the terminal operator weight is $l' = l - d$.

While our algorithm reconstructs these coefficients via tomographic measurements rather than explicit path enumeration, this $l-d$ scaling logic provides a rigorous basis for the sparsity of the dual operator. Crucially, for a fixed precision ϵ , l' remains independent of the depth d because the exponential suppression per layer (Eq. D15)—compounded by noise-induced contraction—effectively counteracts the combinatorial growth of Pauli paths. This synergy ensures that the process information remains physically concentrated in a low-weight Pauli subspace across the entire noise spectrum, fundamentally decoupling the learning complexity from the circuit depth.

Appendix F: Sample Complexity Lower bound for the worst-case scenario

The main manuscript essentially considers learning an efficient classical representation of noisy quantum states and processes in the average-case scenario. As we claimed in Theorems 3 and 4, the tasks of learning noisy quantum states and performing tomography are highly efficient in the average-case setting. However, this does not rule out intrinsic hardness in the worst case. Here we theoretically demonstrate that learning noisy quantum states prepared by quantum circuits subject to constant-strength noise channels is quantum-hard in the worst-case scenario.

The fundamental idea relies on constructing a polynomial reduction to the quantum state discrimination problem.

Task 1. Consider two pure quantum states ρ_0 and ρ_1 , and a noisy quantum circuit \mathcal{C} with depth d , where Each quantum circuit is affected by γ -strength Pauli channel in each layer. Suppose that a distinguisher is given access to copies of the quantum states $\mathcal{C}(\rho_0)$ and $\mathcal{C}(\rho_1)$, then what is the fewest number of copies sufficing to identify these two noisy quantum states with high probability?

Obviously, if one can perform quantum state tomography on these noisy states, then efficient classical representations of the noisy states are obtained. Using these classical representations, one can easily distinguish the noisy states $\mathcal{C}(\rho_0)$ from $\mathcal{C}(\rho_1)$ easily. As a result, Task 1 can be used to benchmark the sample-complexity lower bound for the noisy quantum state tomography problem. We state the result below.

Theorem 5. *Given an unknown noisy quantum state ρ prepared by a d -depth quantum circuit affected by γ -strength local Pauli noise channels, then any algorithm designed to learn an efficient representation to ρ requires at least m samplings in the worst-case scenario, where*

$$m = \frac{(1 - \gamma)^{-2cd}(1 - \eta)^2}{2n},$$

where $c = 1/(2 \ln 2)$ and constant $\eta \in \mathcal{O}(1)$.

When the noise strength $\gamma = \mathcal{O}(1)$, and quantum circuit depth $d \geq \text{poly} \log(n)$, the sample complexity required for quantum state tomography grows at least quasi-polynomially with the system size in the worst-case scenario. We emphasize that this result does not contradict Theorem 3 and 4: the former statement concerns the worst case, while the latter addresses the average case under the random-circuit assumption.

In the quantum process tomography task, when $O > 0$, the target is to learn a classical representation to $\mathcal{C}^\dagger[O]$ which can be easily reduced to a density matrix learning task by setting $\rho = \mathcal{C}^\dagger[O]/\text{Tr}[\mathcal{C}^\dagger[O]]$. This justifies the statement that noisy process tomography (for this observable O) is no easier than state tomography.

To support the proof of our result, we require the following lemmas.

Lemma 8 (Lemma 6 in [94]). *Consider a single instanoise channel $\mathcal{N} = \mathcal{N}_1 \otimes \dots \otimes \mathcal{N}_n$ where each local noise channel $\{\mathcal{N}_j\}_{j=1}^n$ is a Pauli noise channel that satisfies $\mathcal{N}_j(\sigma) = q_\sigma \sigma$ for $\sigma \in \{X, Y, Z\}$ and q_σ be the Pauli strength. Then we have*

$$D_2 \left(\mathcal{N}(\rho) \parallel \frac{I^{\otimes n}}{2^n} \right) \leq q^{2c} D_2 \left(\rho \parallel \frac{I^{\otimes n}}{2^n} \right), \quad (\text{F1})$$

where $D_2(\cdot \parallel \cdot)$ represents the 2-Renyi relative entropy, $q = \max_\sigma q_\sigma$ and $c = 1/(2 \ln 2)$.

Lemma 9. *Given an arbitrary n -qubit density matrix and maximally mixed state $I^{\otimes n}/2^n$, we have*

$$D \left(\rho \parallel I^{\otimes n}/2^n \right) \leq D_2 \left(\rho \parallel I^{\otimes n}/2^n \right), \quad (\text{F2})$$

where $D(\cdot \parallel \cdot)$ denotes the relative entropy and $D_2(\cdot \parallel \cdot)$ denotes the 2-Renyi relative entropy.

Proof: Given quantum states ρ and σ , the quantum 2-Renyi entropy

$$D_2(\rho \parallel \sigma) = \log \text{Tr} \left[\left(\sigma^{-1/4} \rho \sigma^{-1/4} \right)^2 \right]. \quad (\text{F3})$$

When $\sigma = I^{\otimes n}/2^n$, we have $D_2(\rho \parallel I^{\otimes n}/2^n) = \log \text{Tr} \left[\left((I^{\otimes n}/2^n)^{-1} \rho^2 \right) \right] = n + \log \text{Tr}[\rho^2]$. Noting that the function $y = x^2 - x \log x \geq 0$ when $x \in [0, 1]$, and this implies $\text{Tr}(\rho^2) \geq \text{Tr}(\rho \log \rho)$. Finally, we have

$$D \left(\rho \parallel I^{\otimes n}/2^n \right) = n + \text{Tr}[\rho \log \rho] + n \leq \text{Tr}[\rho^2] + n = D_2 \left(\rho \parallel I^{\otimes n}/2^n \right). \quad (\text{F4})$$

Proof of Theorem 5: Now we prove the sample complexity lower bound to the noisy quantum state tomography task. We consider the sample complexity m in distinguishing quantum states $\mathcal{C}(\rho_0)$ and $\mathcal{C}(\rho_1)$. When their trace distance is quite large, let $\eta \in (0, 1)$ and we have

$$\begin{aligned} 1 - \eta &\leq \frac{1}{2} \left\| \mathcal{C}(\rho_0)^{\otimes m} - \mathcal{C}(\rho_1)^{\otimes m} \right\|_1 \\ &\leq \frac{1}{2} \left(\left\| \mathcal{C}(\rho_0)^{\otimes m} - (I_n/2^n)^{\otimes m} \right\|_1 + \left\| \mathcal{C}(\rho_1)^{\otimes m} - (I_n/2^n)^{\otimes m} \right\|_1 \right) \\ &\leq \frac{1}{\sqrt{2}} \left(D^{1/2} \left(\mathcal{C}(\rho_0)^{\otimes m} \parallel (I_n/2^n)^{\otimes m} \right) + D^{1/2} \left(\mathcal{C}(\rho_1)^{\otimes m} \parallel (I_n/2^n)^{\otimes m} \right) \right), \end{aligned} \quad (\text{F5})$$

where the second line comes from the triangle inequality and the third line comes from the Pinsker's inequality. Using Lemmas 8 and 9, we have

$$\begin{aligned} 1 - \eta &\leq \frac{1}{\sqrt{2}} \left(D_2^{1/2} \left(\mathcal{C}^{\otimes m}(\rho_0) \parallel (I_n/2^n)^{\otimes m} \right) + D_2^{1/2} \left(\mathcal{C}^{\otimes m}(\rho_1) \parallel (I_n/2^n)^{\otimes m} \right) \right) \\ &\leq \frac{\sqrt{nm}}{\sqrt{2}} \left((1 - \gamma)^{cd} + (1 - \gamma)^{cd} \right) \\ &\leq \sqrt{2nm} (1 - \gamma)^{cd}, \end{aligned} \quad (\text{F6})$$

As a result we have

$$m \geq \frac{(1-\gamma)^{-2cd}(1-\eta)^2}{2n}. \quad (\text{F7})$$

Appendix G: Additional Experiment result

1. Application: Quantum Error Mitigation

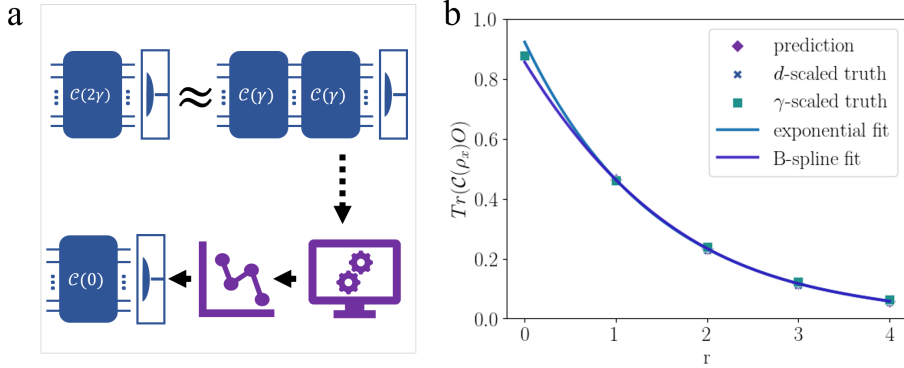


FIG. 3. (a) The procedure of the ZNE. (b) The numerical result of the ZNE-QEM using the proposed learning algorithm.

We note that our learning algorithm can also be applied to solve the quantum error mitigation (QEM) task [13]. QEM comprises protocols that suppress stochastic errors on NISQ hardware by classical post-processing of measurement data, without introducing full quantum error-correcting codes. Whereas error correction aims to eliminate noise, QEM converts every hardware improvement into an immediate fidelity gain by suppressing residual errors. One QEM approach is zero-noise extrapolation (ZNE), which executes the circuit at several circuit fault rates λ , which measures the level of errors occurring in the overall circuit, and $\lambda \propto \gamma$ [95]. Although the circuit output at $\lambda = 0$ cannot be measured directly, an empirical model $h(\lambda)$ linking λ to the circuit output can be built from a set of different λ values. This allows us to extrapolate the case of $\lambda = 0$, which corresponds to zero noise. Different λ values can be generated by pulse-stretching[8, 96] or by inserting additional noise channels [97]. For an i.i.d single-qubit noise, it is natural to set λ proportional to the gate count, thus $\gamma \propto \lambda \propto \text{Number of the gates}$. Here we vary λ by controlling the depth of the circuit d .

Whereas the conventional ZNE must be tailored to each specific input, our protocol is input-agnostic. Similar to Lemma 1, $\text{Tr}(OC(\cdot)) = \sum_{|P| \leq \nu} (1-\gamma)^{|P|} \Phi(\mathcal{C}, P) \text{Tr}(P \cdot)$. Considering the depolarizing noise strength $\gamma < 1$, $(1-\gamma)^{|P|} = (1-\gamma)^{\frac{|P|}{d}d} \approx (1-\gamma d)^{\frac{|P|}{d}}$. In other words, one can obtain the characterizations of the same quantum processes with different noise strength by appending extra quantum circuit layers to the original process, this yields a sequence of learned values $\{f_r | |f_r - \text{Tr}[OC_{rd}(|0^n\rangle\langle 0^n|)]| \leq \epsilon\}_{r \geq 1}$. One can utilize $\{f_r\}_{r \geq 1}$ to extrapolate f_0 , which is considered as the characterization of \mathcal{C}_d with zero noise.

The result of numerical experiments of application is shown in Fig 3, where we simulate a six-qubit 2D transverse field Ising model

$$H = -J \sum_{\langle q,p \rangle} Z_q Z_p + h \sum_q X_q, \quad (\text{G1})$$

with 5 layers. Two key observations emerge:

- Rescaling either the depth coefficient d or the noise strength γ perturbs the dynamics to a comparable extent, as seen from the nearly overlapping dots.
- The characterization obtained by learning the coefficients of d can be extrapolated via curve fitting to estimate the noise-free system (i.e., when $\gamma = 0$) characterization. Exponential extrapolation yields an error 0.0446; a cubic B-spline (piecewise polynomial) reduces it to 0.0222.

2. numerical experiment for highly entangled input state

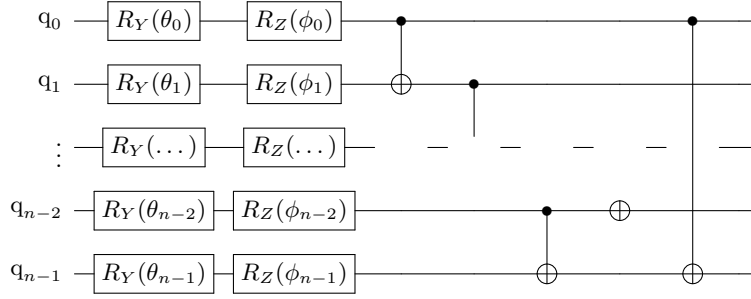


FIG. 4. The demonstration of a layer of the state preparation circuit for n qubits. The structure consists of parameterized single-qubit rotations followed by a cyclic CNOT entangling layer.

To further underscore the novelty of our **input-agnostic regime**, we constructed a Quantum Process Tomography (QPT) experiment using an input state that is **highly entangled** and falls outside the distribution set addressed by previous work [67]. The method detailed in [67] requires the input distribution to be at most polynomially far from a **locally flat distribution**.

As demonstrated by [67], locally flat distributions encompass: Random product states, ground and thermal states of random local Hamiltonians and any state generated by a circuit whose final layer consists of random single-qubit gates.

Here, we intentionally generated the input state ρ_x using a two-layer parameterized circuit to ensure high entanglement. Each layer of this state preparation circuit is structured as depicted in Fig. 4.

The experimental result of performing QPT with this highly entangled input state is presented in Fig. 5. The outcome clearly demonstrates that **our algorithm's performance is not constrained by the entanglement level or specific structure of the input state**, thus validating its input-agnostic nature.

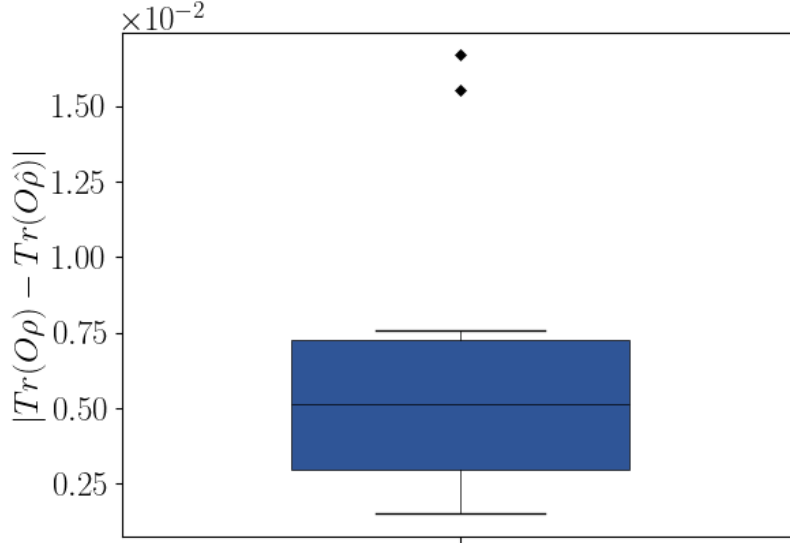


FIG. 5. The experiment result of QPT where the input state is generated from the form as Fig. 4. Set $l' = 2$ and the process Eq. G1 with 5 layers is at the depolarizing noise strength 0.01.

3. full matrix figure

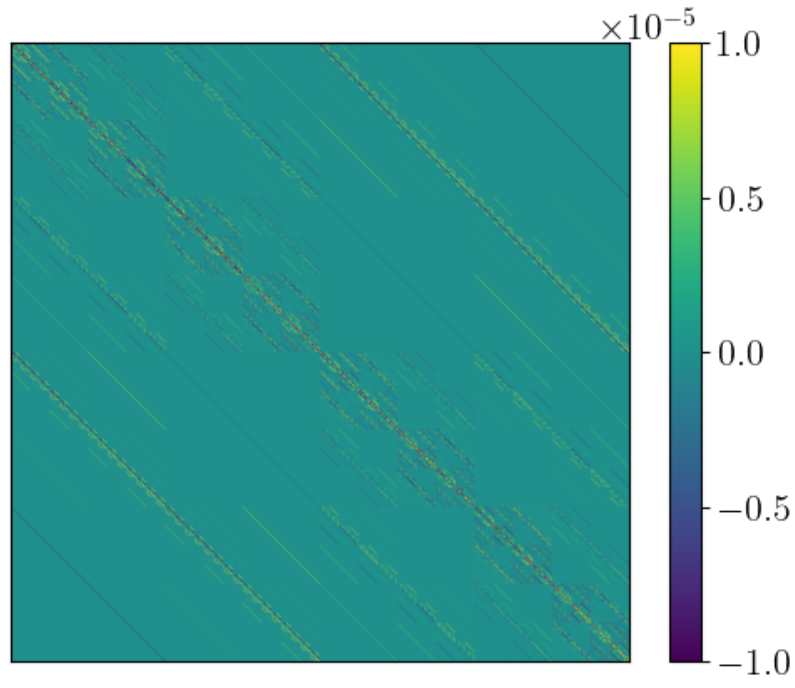


FIG. 6. The heatmap visualizes the full matrix of the $\tilde{\rho} - \hat{\rho}$ in Fig 2 c, when $\theta_h = \frac{\pi}{2}$.